





Article

Interaction of Polyoxometalates and Nanoparticles with Collector Surfaces—Focus on the Use of Streaming Current Measurements at Flat Surfaces

Johannes Lützenkirchen ^{1,*} , Gopala Krishna Darbha ^{1,2,*},
Venkata Sai Kiran Chakravadhanula ^{3,4,†} , Engelbert Redel ⁵, Atida Selmani ⁶  and
Lionel Vayssières ⁷ 

- ¹ Institute for Nuclear Waste Disposal, Karlsruhe Institute of Technology (KIT), Hermann-von-Helmholtz-Platz 1, D-76344 Eggenstein-Leopoldshafen, Germany
- ² Department of Earth Sciences & Centre for Climate Change and Environmental Studies, Indian Institute of Science Education and Research Kolkata, Mohanpur 741246, West Bengal, India
- ³ Helmholtz Institute Ulm (HIU), Electrochemical Energy Storage, Helmholtzstr. 11, 89081 Ulm, Germany; cvskiran@gmail.com
- ⁴ Karlsruhe Nano Micro Facility (KNMF), Karlsruhe Institute of Technology (KIT), Hermann-von-Helmholtz-Platz 1, D-76344 Eggenstein-Leopoldshafen, Germany
- ⁵ Institute of Functional Surfaces (IFG), Karlsruhe Institute of Technology (KIT), Hermann-von-Helmholtz-Platz 1, D-76344 Eggenstein-Leopoldshafen, Germany; engelbert.redel@kit.edu
- ⁶ Division of Physical Chemistry, Laboratory for Biocolloids and Surface Chemistry, Ruđer Bošković Institute, Bijenička c. 54, 10000 Zagreb, Croatia; aselmani@irb.hr
- ⁷ International Research Center for Renewable Energy, State Key Laboratory of Multiphase Flow in Power Engineering, Xi'an Jiaotong University, 28 Xianning west road, Xi'an 710049, China; lionelv@xjtu.edu.cn
- * Correspondence: johannes.luetzenkirchen@kit.edu (J.L.); gkdarbha@gmail.com (G.K.D.)
- † Presently at Materials and Metallurgy Group, Materials and Mechanical Engineering Entity, Vikram Sarabhai Space Centre, Thiruvananthapuram 695022, India.

Received: 12 May 2020; Accepted: 26 August 2020; Published: 8 September 2020



Abstract: Streaming current measurements were used to study the interaction of polyoxometalates (POMs) and nanoparticles (NPs) with flat surfaces as an alternative, innovative approach to infer POM and NP properties of potential sparse material in terms of charge and magnitude. With respect to POMs, the approach was able to reveal subtle details of charging properties of +7 vs. +8 charge at very low POM concentrations. For NPs, the sign of charge and even the zeta-potential curve was retrieved. Concerning NPs, mutual interaction between TiO₂ and SiO₂ surfaces was studied in some detail via macroscopic measurements. Post-mortem analysis of samples from electrokinetic studies and separate investigations via AFM and HRTEM verified the interactions between TiO₂ NPs and SiO₂ collector surfaces. The interactions in the SiO₂/TiO₂ system depend to some extent on NP morphology, but in all our systems, irreversible interactions were observed, which would make the studied types of NPs immobile in natural environments. Overall, we conclude that the measurement of streaming currents at flat surfaces is valuable (i) to study NP and POM collector surface interactions and (ii) to simultaneously collect NPs or POM (or other small mobile clusters) for further (structural, morphological or release) investigations.

Keywords: polyoxometalates; nanoparticles; DLVO; SiO₂; TiO₂

1. Introduction

1.1. Background

Nanoparticles (NPs) are entering the environment, largely unnoticed by the general public, although scientific investigations are numerous and the concern for potential adverse effects on human health need not even be referenced.

The use of engineered NPs in science and technology arises from a strong interest in the surface properties of NPs. The NPs emerging in nature are expected to cause adverse effects in various compartments of the environment [1–8]. Among the most important groups of such emerging materials are TiO₂ NPs. Various aspects of NP physico-chemical behavior or transport processes have been addressed, including the role of air–water interfaces [9], the effect of UV radiation [10], the desorption of adsorbed metal ions that can be transported by TiO₂ NPs [11], and the respective influences of natural organic matter [12] or surfactants [13], to name only a few. Overviews addressing the role of TiO₂ NPs in the environment concerning processes and modelling have been published by Ju-Nam and Lead [14], Petosa et al. [15], Goldberg et al. [16], and Schaumann et al. [7], with this list being by no means complete. Since NPs are emerging in so many environmentally relevant contexts, simple methods for detecting and characterizing NPs are required.

Within this broad area of research, the present study partially focuses on the interaction of NPs with collector surfaces in relation to NP transport in the environment, be it as intrinsic NPs or as NPs attached to other (larger) particles or agglomerates. In the latter case, the detachment of the NPs from the collector substrates is of interest. For example, if the larger particles are retarded or retained in a porous medium (due to size), smaller particles when detached may regain mobility. In NP-transport and other contexts, the interactions of various sub-micrometer particles with surfaces have been studied [17–21]. Moreover, TiO₂ NPs have been the subject of various kinds of hetero-coagulation experiments [22,23]. The study of such interaction frequently involves electrokinetics and adhesion isotherms, but also light scattering and direct force measurements. In one case where the interaction of small SiO₂ colloids with larger TiO₂ particles was studied [22], it was observed that the composite electrokinetic behavior of the system turned towards that of SiO₂ when the weight ratio of SiO₂ to TiO₂ was about 0.5 g/g. In another case, adhesion isotherms of small TiO₂ on larger SiO₂ particles were reported [23]. In that study, a strong effect of the pH on the uptake was observed up to a pH of 6 (the typical isoelectric point, IEP, of TiO₂), whereas above this pH, where both surfaces were negative, the uptake became independent of pH. The resulting composites were not further studied. In a different context, composite TiO₂-SiO₂ particles have, e.g., been prepared via evaporation methods [24] because of their photocatalytic activity [25]. In aqueous solution the behavior of such composites may be highly complex, and properties such as the point of zero charge of mixed oxides are of fundamental interest [26–30]. The mutual electrostatic potential effects involve charge regulation, the extent of which will depend on the size of the patches generated by the pattern that evolves when one oxide is fixed on the supporting surface [26,31].

Compared to colloids and NPs, the interaction of polyoxometalates (POMs) with collector surfaces appears to be much less explored. POMs are small inorganic polymeric species that can be seen as intermediates between solutes and NPs. They share properties with either of them but also show behavior that is unique [32,33]. The interaction of small Keggin-ions with surfaces was pioneered in the thesis of Hernandez [34], who systematically studied the interaction of some Keggin-ions with various oxidic minerals and highlighted chemical similarities among Al-based Keggin-ions and gibbsite basal planes, which led him to interpret their mutual interactions from a structural point of view. Overall, strong interaction was observed, even between strongly positively charged Al₁₃ entities and positively charged collectors.

Since we are interested in both the oxide mineral and POM electrolyte interfaces, the remainder of the introduction addresses relevant details on oxide–electrolyte interfaces and subsequently on the

aqueous chemistry of the Al_{13} type Keggin ions of interest, before introducing the methods used in this work and finally defining the aims of the study.

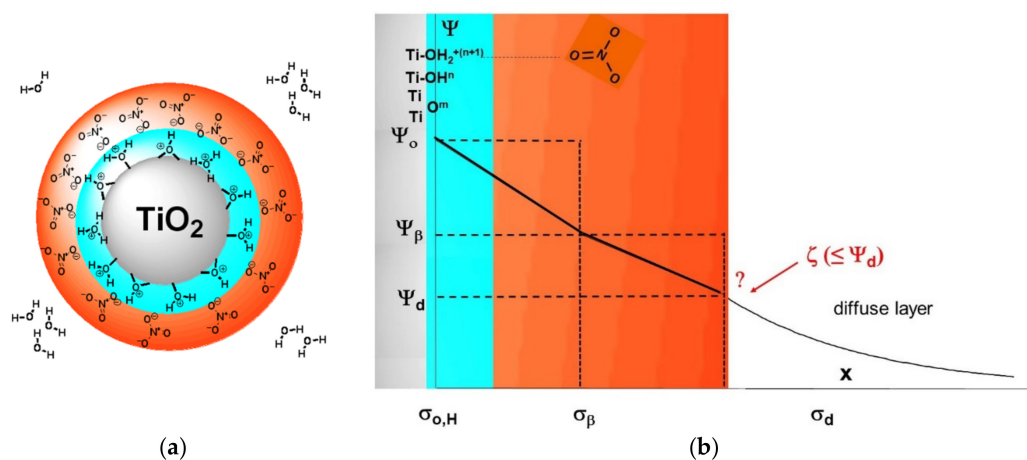
1.2. Short Survey of Oxide–Electrolyte Interfaces

The behavior of oxide surfaces in aqueous electrolyte solutions has been the subject of many investigations. A major property of a given interface is the pH at which the interface is net uncharged. Depending on the method used to obtain this pH it may be referred to as isoelectric point (noted IEP and referring to the zero point of charge based on an electrokinetic method) or as point of zero net proton charge (noted PZNPC and referring to the zero point evaluated from potentiometric or mass titrations). The particles assume a positive charge below such a point of zero charge and a negative charge above. This is, in oxidic minerals, at the fundamental level caused by the uptake or release of protons by surface functional (hydroxyl) groups. For a given pH below the PZNPC net proton uptake is favored when the salt content in the suspension increases. The increase in salt concentration concomitantly causes stronger shielding of the fundamental charge, which in a somewhat counter-intuitive way decreases the net-charge within the slip plane (the sum of the fundamental charge brought to the surface by proton adsorption and the opposite charge brought to the interface by counter-ions, i.e., anions for $\text{pH} < \text{IEP/PZNPC}$). Originally, such properties of particles in suspension were studied in colloids, which already included particles that are nowadays called NPs.

Therefore, bare, uncoated NPs in terms of surface charging behave in many ways as classical colloids. In practice, many NPs in suspension as supplied by manufacturers will be stabilized against aggregation, often by a layer of organic material, typically surfactants [35]. In our study, we exclusively use purely inorganic NPs without organic stabilizers. Colloidal stability of products from surfactant-free synthesis routes typically originates from the above-mentioned surface functional groups, which form charged surface-species. In TiO_2 stock suspensions (such as those we are using), a pH below the IEP is imposed, such that positively charged surface groups dominate (Scheme 1a). These are partially neutralized by a layer of counter-ions (for example nitrate ions, NO_3^-). In the present context this causes sufficient positive charge via dominant site protonation ($\text{pH} < \text{IEP}$ by HNO_3 addition, for $\text{pH} > \text{IEP}$ net deprotonation yields negative surface charge), which results in sufficient kinetic stability against agglomeration. Sufficient excess of positive charge (or low pH) assures repulsive electrical double layer forces (according to the DVLO theory) between the NPs which limits aggregation. Scheme 1b shows the electrical double layer, here a triple layer model [36,37], for the particle in Scheme 1a. The surface potential (Ψ_0) is a consequence of the adsorption (or the release) of protons to surface functional groups which is characterized by the measurable surface charge density ($\sigma_{\text{o,H}}$) via potentiometry. The interfacial potential decays towards the solution with a linear decrease in the Stern layer and an exponential decay in the diffuse layer. The fundamental charge ($\sigma_{\text{o,H}}$) is partially screened by the adsorption of counter-ions in the Stern layer. The remaining excess charge is neutralized in the diffuse part of the double layer. The measurable zeta-potential (ζ) pertains to at an unknown position close to the onset of the diffuse layer. It corresponds to the potential at the plane of shear, which divides the part of the interface that sticks to the surface (i.e., the layers of water and ions that move with the particle in an applied electric field, or remain immobile under an applied pressure in a streaming potential experiment). The interactions of particles among themselves or with collector surfaces (aggregation, stabilization, deposition) are governed by solution chemistry (pH, ionic strength, general known solution composition, and impurities), particle morphology (surface topography), surface roughness or even, if applicable, hydrodynamic (flow velocity) parameters.

There is common agreement that primary effects on surface charging of oxide minerals occur via changes in (i) pH (changing the charge in terms of sign and magnitude due to protonation and deprotonation of surface functional hydroxyl groups), (ii) ionic strength (fixed by simple, ideally inert, background electrolyte salts, that only screen, where increased salt levels favor screening and interaction between like-charged particles), and (iii) specifically adsorbing solutes (other than proton

and hydroxide affecting IEPs and changing the behavior more dramatically beyond simple screening, including overcharging or charge reversal).



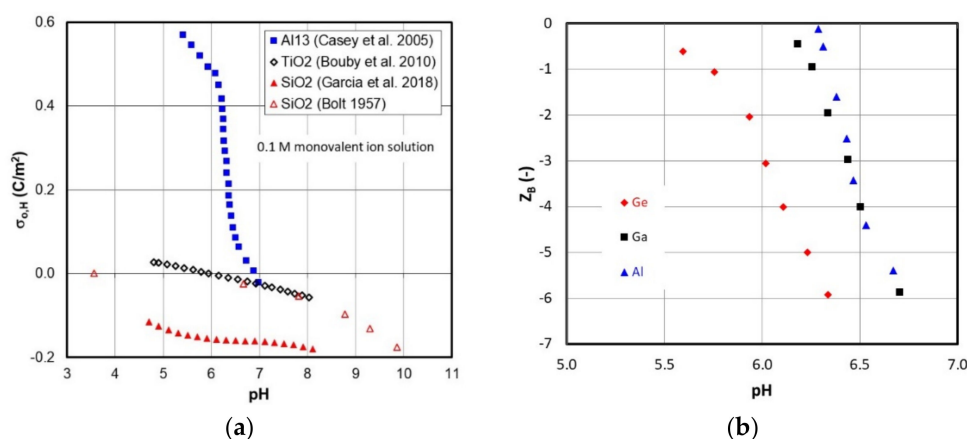
Scheme 1. (a) Schematic drawing of a charge stabilized TiO₂ NP in acidic HNO₃ solution. (b) Electrical double layer around the particle sketched in (a). The zeta-potential (ζ in the scheme) is at located at some unknown position (indicated by “?”) close to the onset of the diffuse layer.

To define optimum conditions for NP aggregation, for example, the fundamental surface charge density due to proton interaction, zeta-potentials and IEPs have to be measured for any relevant set of particles, since nominally identical particles may have different IEPs due to differing origin (e.g., varying synthesis procedures). In more complex situations, properties of the solution (i.e., temperature, potential presence of specifically adsorbing ions, etc.) will affect interfacial electrostatics. Apart from the electrostatic contribution due to interacting double layers classical DLVO theory involves attractive short range (van der Waals) forces. Phenomena beyond classical DLVO theory may also be at play [17,38].

1.3. Short Survey of MeAl₁₂-Keggin Acid–Base Chemistry

The approximately 1-nm Keggin-ions considered in the present work are polyoxometalates (POMs). Structural properties of the substrates have been summarized by Casey [39]. The ϵ -Keggin ions [AlO₄Al₁₂(OH)₂₄(OH₂)₁₂]⁷⁺ (referred to as Al₁₃), [GaO₄Al₁₂(OH)₂₄(OH₂)₁₂]⁷⁺ (GaAl₁₂), and [GeO₄Al₁₂(OH)₂₄(OH₂)₁₂]⁸⁺ (GeAl₁₂) will be denoted as MeAl₁₂, where Me represents the cation in the tetrahedral unit in the center of the Keggin-ion. The three compounds have been extensively studied in terms of acid–base behavior in aqueous electrolyte solutions [32,33,40]. Results are shown in Scheme 2a for Al₁₃ in terms of surface charge density in comparison to typical data for the two oxides used in the present study. Clearly, the surface charge density is much higher on Al₁₃. Moreover, we emphasize that for silica type surfaces at least two distinctly different surface charge curves can be found in the literature. One involves a single deprotonation step (Bolt-type), with no significant charge from silanol deprotonation below pH 5, while the other exhibits two deprotonation steps. The TiO₂ curve in Scheme 2a exemplifies the behavior of most oxide minerals with a sharp point of zero charge resulting in positive and negative charge densities in the common pH ranges.

Scheme 2b shows the distinct effect of charge on the Keggin-ions as a function of pH in terms of Z_B. Z_B is defined as the number of protons reacted per Me, where Z_B = 0 corresponds to the maximum charge of a given ion, i.e., +8 for Me = Ge, and +7 for Ga and Al. One Z_B unit corresponds to the release of one proton from a Keggin-ion. At Z_B = −7 the Al/Ga polymorphs are uncharged, while the Ge polymorph has a +1 charge. The deprotonation is extremely steep (i.e., much steeper than for oxide minerals, see Scheme 2a), and GeAl₁₂ with its +8 charge deprotonates at lower pH than the other two, which behave more or less identically. The +8 charge at pH < 5 leads to about 14 per cent higher charge density on GeAl₁₂ compared to Al₁₃ (Scheme 2a).



Scheme 2. (a) Acid–base properties of ϵ -MeAl₁₂ Keggin-ions in relation to oxides: Surface charge density of Al₁₃ [39], TiO₂ [41] and SiO₂ [42,43] as a function of pH in 0.1 M monovalent electrolyte concentration. (b) Acid–base behavior of ϵ -MeAl₁₂ Keggin-ions compared to each other [33]: Z_B (i.e., the amount of protons released per Me unit) as a function of pH for Me = Ge (+8 charge), Me = Al (+7 charge) or Me = Ga (+7 charge). TOTMe is 12.5 μ M and 0.1 M monovalent electrolyte concentration is used as background electrolyte.

In summary, the Keggin-ions investigated in the present work may exhibit proton related charge densities significantly higher than typical oxide minerals. Furthermore, their deprotonation occurs in a very narrow pH interval, again different from oxide minerals which in most cases deprotonate over all the pH range accessible to pH measurements.

1.4. Corollary of Methods Applied and Systems Studied in the Present Work

Classical colloid chemistry techniques to obtain information about surface charging involve to a large extent potentiometric acid–base titration [44] and electrophoretic mobility measurements [45]. The former yields primary proton uptake and release, on a relative scale (ultimately, this technique yields $\sigma_{o,H}$ or Z_B , i.e., data shown in Scheme 2). The latter yields absolute values of the typically published zeta-potentials as obtained from fundamental data (in most cases electrophoretic mobility, i.e., the particle velocity divided by the applied electrical field).

Besides the more frequently used determination of zeta-potential via scattering techniques, the present work mainly involves streaming current measurements at flat surfaces [46]. The determination of zeta-potential of flat collector surfaces covered by NP layers via streaming current measurements were inspired by previous work on adhesion techniques involving porous media [47], where the breakthrough of a particle suspension through a column of larger beads with a given charge at the respective pH value was observed. By changing the pH and thus the charges of the collector and the suspended particles, it was possible to infer the IEP of the suspended particles. Similar studies with flat surfaces have been reported to obtain the IEP of the flat surface based on the knowledge of the IEP of the added NPs [48] using a rotating-disk method. In work by Adamczyk and co-workers, adhesion of particles on flat surfaces was previously studied via streaming potential: examples involve mica as a collector surface [49,50], including oxides as added particles [51]. No direct comparisons between the properties of the added particles prior to and the properties of the collector surfaces after the addition of the particles was available. In general, with the appropriate set-up, the changes in the streaming potential of the supporting (collector) surface resulting from the addition of NPs can be directly measured, and the idea was to try and correlate the composite zeta-potential of the binary system TiO₂ NP/SiO₂ collector to the independently determined zeta-potential of the TiO₂ NPs for the same solution composition.

A second series of experiments aimed at verifying to what extent interactions between the studied surfaces (SiO₂ and TiO₂ polymorphs, see Scheme 2a for typical charging curves ($\sigma_{o,H}$) of

these substrates) can be generalized, because we observed irreversible interactions (aggregation, adhesion), as well as adhesion under conditions when both surfaces were negatively charged. For this aspect, different TiO₂ NPs were used that varied in properties due to the method of preparation, i.e., had different morphology. More specifically, the interactions among TiO₂ NPs with SiO₂ collector surfaces, quartz (001) single crystal surfaces and amorphous SiO₂ colloids, were studied by streaming current and electrophoretic mobility, respectively [52,53]. This was completed by interacting SiO₂ NPs with flat TiO₂ surfaces via streaming current.

In the first part, the streaming current measurements at flat surfaces involved the study of the Keggin-ions discussed in Section 1.3 with flat surfaces to learn about the sensitivity of the technique to slight changes in charge of the added material in more detail than previously reported [54]. The Keggin-ions can be seen as proxies for nuclear waste related radioactive polymeric species which have been found to be mobile, but difficult to study in terms of charge [55,56].

1.5. Aims of the Study and Strategy

The initial aim of the work was to test to what extent streaming current measurements (i.e., the determination of zeta-potentials) at flat surfaces in the present study can access systems (with POMs and NPs as target compounds) that might be otherwise difficult to characterize in terms of charge. Thus, the Keggin-ions of different charge as proxies for Eigen-colloids of radionuclides that form small polymers [57] were used to show how sensitive the method is. Likewise, we use the approach to study the charging of NPs/colloids. This is similar to experiments by Morga et al. [58] on even more complex systems, where at constant pH bilayers of hematite and silica were studied on mica (i.e., a ternary particle system). Here, we perform such experiments on binary particle systems, but we (i) typically vary the pH to (a) identify the IEP and (b) to compare it to the IEP of the target compounds, and (ii) exchange the role of collector and target surface. In the course of the experiments, we became interested in the non-reversibility of the interaction in the SiO₂/TiO₂ system and attempted to gain more information as to whether observed persistence under like charge conditions can be generalized. Ideally, the number of particles deposited on the support in such systems should be quantified in particular if one wants to draw conclusions about the surface coverage. This is also done in more fundamental research where the coverage is quantified by imaging or via separate experiments in much more detail than in the present work [51,58–60]. In the present study, we emphasize that the total amount of particles added to a given collector is not necessarily the amount of deposited particles. Our goal was to gain insight in the total amount required to produce the properties of the adsorbing particles or to show the sensitivity of the approach to small differences in the charge of the Keggin-ions or the collector surface.

Concerning terminology, we note that by “unfavorable conditions” for interaction between particles we will here understand conditions that correspond to surfaces of like charge irrespective of charge density, interfacial potential or electrolyte concentration. For unlike charge, we may expect that adhesion will occur irrespective of salt level for example. For like charges the situation is more complicated because particles with like charge may aggregate at sufficiently low surface charge (for example close to the IEP) and also at sufficiently high salt concentration with high surface charges.

2. Materials and Methods

2.1. Solutions

Aqueous solutions were prepared from MilliQ water that had been bubbled with purified Ar to remove carbon dioxide. The Ar gas was purified via washing bottles consisting of sodium hydroxide solution (to strip off residual carbon dioxide in the Ar) and medium solution (to minimize water evaporation from the solutions). Salt solutions were prepared from dried salt. Dilute NaOH or KOH and HNO₃ or HCl solutions were used to adjust the pH. No buffers were used to fix pH values. All chemicals were obtained from VWR and were analytical grade.

2.2. Materials

2.2.1. Nanoparticles

Three kinds of TiO₂ NPs (Samples A–C) were used. The synthesis of Sample A will be briefly described below. The preparation of Sample B has been previously described in detail [61], and some characterization of the resulting NPs is available [62]. Samples A and B are comparable in terms of size, while Sample C involves nanowires (NWs) with different shape and size compared to the two other samples. A separate batch of Sample C has previously been extensively characterized [63] and studied in some detail. The SiO₂ NPs were commercial products. In the following, relevant details of the synthesis of the TiO₂ NPs and the sources of the SiO₂ NPs will be given.

TiO₂ Nanoparticles

Sample A: The preparation of Sample A TiO₂ NPs was carried out via controlled aqueous precipitation without surfactant [64]. Primary NPs are on the order of a few nanometers on average diameter and are charge-stabilized in their acidic stock suspension/dispersion, but are expected to agglomerate to some extent in salt solutions and/or at changed pH conditions. In the present work, specific characterization of the bare stock suspensions was done by AFM and TEM after deposition on a mica surface or a carbon-coated Au grid, respectively.

Sample B: The preparation of the charge stabilized sample [61] was carried out by drop-wise addition of Titanium iso-propoxide, TTIP, ($w = 98\%$, for synthesis, 17.5 mL) to 108 mL of a 0.1 M HNO₃ solution at room temperature under vigorous stirring. After adding the TTIP precursor the resulting suspension was stirred for 8 h at 80 °C. The synthesis is finished when a fine white-milky dispersion is observable. The respective dispersion was allowed to cool down to room temperature (RT) and possible impurities or remains of unreacted Ti-precursor were removed by a paper filter. The final dispersion is long-term stable and can be stored at RT in brown bottles.

Sample C: The TiO₂ NWs were prepared hydrothermally similar to a procedure published by Kasuga [65]. Briefly, a mass of 2 g TiO₂ powder (P-25 Degussa, Degussa, now Evonik, Essen, Germany) was added to 65 mL of 10 molar NaOH aqueous solution. The resulting suspension was stirred for 3 h under Ar and ultrasound and then transferred to a PTFE-lined autoclave and heated at 190 °C for 24 h. The obtained precipitate was filtered and washed with deionized water until pH remained close to 6.5 for at least two subsequent washing steps. The sample was then magnetically stirred for three hours in 0.1 M HCl to remove excess sodium, filtered and washed with deionized water repeatedly until pH remained close to 7 and conductivity was close to that of de-ionized water (<10 µS/cm). The TiO₂ NWs were dried at 80 °C for 6 h in air and finally stored in a glass bottle. Since one dimension of the otherwise rather large TiO₂ NWs is below 100 nm, we refer to this sample as NPs.

SiO₂ Nanoparticles

Two kinds of SiO₂ NPs were used. Ludox TMA was obtained from Sigma Aldrich (Munich, Germany). Aerosil OX 50 was obtained from Degussa. Both products were used as received.

Selected properties of all NPs are summarized in Table 1.

Differences in the primary particle size and the measurements in suspension are not unusual and are caused by aggregation of the primary NPs.

Table 1. Properties of the nanoparticles used in the present work.

	TiO ₂ NP A	TiO ₂ NP B	TiO ₂ NP C	SiO ₂ NP A	SiO ₂ NP B
Source/Reference	Synthesized [64]	Synthesized [61]	Synthesized [63]	LUDOX TMA Sigma Aldrich	Aerosil OX 50 Degussa
Primary particle size	<5 nm	4–8 nm	50–300 nm (diameter) 500–300 nm (length)	22 nm	40 nm
Size from measurements in suspension	60 nm	30–60 nm	NA	40 nm	450 nm
IEP (electrophoresis)	4.4–5.1	6.1	3.6	<3	1.0

2.2.2. Keggin-Ions

Solutions of Keggin-ions were prepared according to published recipes [32,33]. The resulting solutions were not crystallized (as selenate or sulfate salts) but directly used as crude solutions as in other studies [40,66,67]. The solutions are dominated by the Al_{13}^{7+} , GaAl_{12}^{7+} , and GeAl_{12}^{8+} Keggin-ions with minor amounts of unreacted Al monomers or dimers. The interest is here in the fact that the Ge-polymorph has a slightly higher charge (+8) in its natural form compared to the +7 charges of the two other polymorphs. Work on the Keggin-ions was carried out in sodium chloride solutions with HCl and NaOH to adjust the pH.

2.2.3. Collector Surfaces

Quartz (001) single crystals were obtained from Mateck (Jülich, Germany). The 20 mm by 10 mm substrates, epi-polished on one side by the supplier, as all other single crystals, were cleaned following a procedure previously established for sapphire-c single crystals [68]. The quartz (001) samples were used as collector surfaces for the TiO_2 NPs. Their charging behavior has been studied previously [69,70].

Rutile (TiO_2) single crystals exposing the (001) face, obtained from TBL Kelpin (now Mateck), were used as collector surfaces for interaction with SiO_2 NPs (Ludox TMA, Sigma Aldrich, Munich, Germany).

For the interaction with Keggin-ions a set of sapphire-c crystals (i.e., the 001 plane) and a set of fused SiO_2 single crystals were used as collector surfaces. The crystals were obtained from TBL Kelpin (now Mateck). The sapphire-c samples have been previously studied by streaming current/potential approaches [54,68,71].

For some of the separate size measurements using AFM, freshly cleaved mica sheets (Sparsh Mica Co., Giridih, Jharkhand, India) were used.

2.3. Experimental Procedures and Methods

All measurements were carried out at RT. Details on the preparation of solutions, the synthesis, origin and treatment of the NPs and the origin and cleaning of the single crystal systems were included in the previous sections.

2.3.1. Electrophoretic Mobility Measurements

Classical electrokinetic measurements involving NPs were done using the Brookhaven PALS apparatus. The data were obtained in simple electrolyte solutions (concentration typically 1 mM) under inert gas N_2/Ar atmosphere. Additionally, data in 10 mM NaNO_3 medium were collected for Sample A TiO_2 NPs, since the location of the IEP needed to be established more rigorously. Data for Sample C have been previously published [64], and the new data agree well with those. The results for the bare SiO_2 colloids are presented as electrophoretic mobility, mainly because the range of ionic strength varies over three orders of magnitude between the starting values at alkaline pH (dominated by 1 mM NaNO_3 or KCl) and the isoelectric point at pH 1 (dominated by 100 mM HNO_3 or HCl). Care was taken to avoid mixed electrolyte solutions, i.e., the anions nitrate/chloride and cations potassium/sodium were never mixed. The main interest of these measurements is to determine the IEP.

The measurements were started from suspensions at low pH. Suspensions of Samples A and B were charge stabilized at low pH, while suspensions of Sample C were initially adjusted to low pH. Low pH facilitates removal of carbon dioxide. Subsequently, NaOH solution was added to the aqueous suspensions to gradually increase the pH, whereupon the suspensions were left to equilibrate for at least 10 min. During the experiment, a stream of inert gas flowed over the suspension. Empty cuvettes for the zeta-potential measurements were flushed with Ar and after filling with the appropriate volume of suspension the cuvettes were contacted with Ar again by a stream of purified Ar over the cuvette prior to inserting the measurement cell. The measurement device was also kept under Ar.

Electrophoretic mobilities of mixed TiO₂ (Sample A) and Aerosil OX 50 suspensions were determined in 1 mM NaNO₃ at distinct pH values as a function of TiO₂/SiO₂ ratios. TiO₂ NPs were added to SiO₂ suspensions. Procedures were as described above. Zeta-potentials were, when required, calculated using the Hückel equation.

2.3.2. Determination of Zeta-Potential at Flat Surfaces

The determination of zeta-potential at flat surfaces was carried out via streaming current measurements on quartz (001) surfaces in 1 mM NaNO₃ in the absence and presence of Sample A TiO₂ NPs. NaOH and HNO₃ solutions were used to adjust the pH. Additional measurements were done on the rutile (001) surface in 1 mM KCl in the absence and presence of Ludox TMA SiO₂ NPs (at pH 4.1). pH-scans in this system were done using KOH and HCl solutions. Furthermore, experiments with the Keggin-ions on sapphire-c and fused SiO₂ single crystals were carried out either at constant pH and ionic strength for increasing Keggin-ion concentration or at a given Keggin-ion concentration and constant ionic strength as a function of pH in 1 mM NaCl involving appropriate acid and base solutions (HCl and NaOH). All these measurements were performed with the SurPass apparatus (Anton Paar) using the gap-cell, which operates at a rectangular flow channel with a height of about 100 µm. A schematic presentation of the set-up is shown in Scheme 3 in an exemplifying way for the TiO₂ NP/quartz system. The experiments were typically started at low pH by adding a small amount of NP suspension (100 µL of 1 g/L suspension) to a solution (500 mL) containing 1 mM NaNO₃ and HNO₃ to obtain pH about 4. Then an automated pH titration by NaOH solution (50 mM) was started. The equilibration time in the zeta-potential measurements was 10 min for each pH. Six pressure ramps were recorded for each pH and no transient behavior was observed during data collection at a given pH, which suggests that a steady state was obtained in all cases under the chosen experimental conditions. At the end of the titration (i.e., pH 7) the quartz (001) samples were dismantled and used for AFM measurements. The zeta-potential measurements with the other single crystals were carried out in the same way. The measurements were carried out as streaming current measurements to avoid problems related to surface conductivity. The zeta-potentials were calculated from the measured quantity (i.e., current ramps dI/dp) by the formula

$$\zeta = \frac{dI}{dp} \times \frac{\eta}{\varepsilon \times \varepsilon_0} \times \frac{L}{A}$$

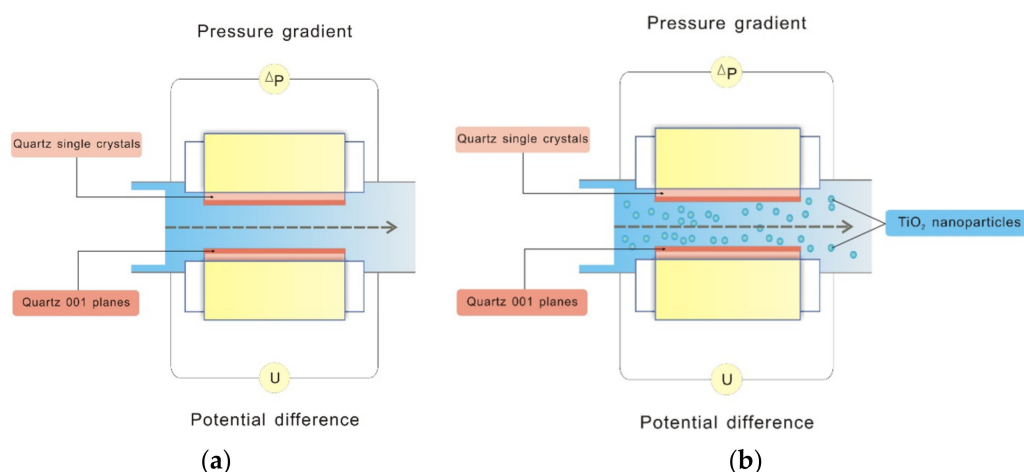
where ζ is the zeta-potential, η is the electrolyte viscosity, ε_0 is the vacuum permittivity, ε is the dielectric constant of the electrolyte solution, L is the length of the channel (20 mm) and A is the cross-section of the channel (10 mm × 100 µm). The built-in software accounts for the temperature dependence of the solution properties. Temperature, pH, and conductivity are constantly monitored by the software.

2.3.2.1. pH Measurements

For the conventional electrokinetic experiments pH measurements were carried out using Ross-Orion or Orion 720 electrodes and an Orion 720 A+ pH meter (Fisher Scientific) or a Metrohm system (microelectrode 6.0234.110 and 827 pH meter). The pH measurement set-ups were calibrated using commercial pH buffers (ranging from pH 2–10) on the millivolt scale. The pH measurements in the SurPass apparatus were done using the built-in device, involving a Schott BlueLine 15 pH electrode. The calibration on the pH scale involved three commercial buffers (3, 6 and 9) via the SurPass internal procedure.

2.3.2.2. Size Measurements

Size determination for Sample A NPs diluted in a 1 mM NaNO₃ solution was done by the Brookhaven apparatus. Additional size measurements were carried out using the Brookhaven apparatus with NPs in MilliQ water and by AFM and TEM as described below. Information on the size of the different NPs is summarized in Table 1.



Scheme 3. Scheme of the gap-cell for determining zeta-potentials at flat surfaces, here as streaming potentials, (a) for the quartz (001) plane and (b) for the quartz (001) plane in the presence of the TiO_2 NPs. For streaming current measurements, the set-up measures the current generated by the movement of liquid through the channel.

2.3.2.3. AFM and TEM Measurements

These methods were selectively used for size characterization of NPs in their original state and on the collector surfaces but also to verify NP collector interactions. AFM measurements were carried out in contact mode using a dimension 3100 (Bruker, Ettlingen, Germany) equipped with a Nanoscope IV controller. Studies were carried out with the TiO_2 (Sample A NPs) on the quartz (001) collector surfaces after the end of the zeta-potential measurements, i.e., for samples retrieved at pH 7. Some additional tests were done with freshly cleaved mica planes instead of quartz (001) planes, since the former are much cheaper. The cleaved mica planes have a negative zeta-potential (similar to SiO_2 surfaces).

Additional AFM studies were undertaken to test the reversibility of interactions. In such experiments as an example a volume of Sample A TiO_2 NP suspension with known pH was added to quartz (001) surfaces under unlike and like charge conditions based on the known IEPs of the surfaces involved. These tests were carried out, after experiments with TiO_2 Sample A NPs had shown that the latter (i) were not removed from quartz (001) at pH 7, and (ii) interacted with amorphous SiO_2 under unfavorable conditions. The intention was to confirm that NPs indeed adhered to the collector surface. Subsequently, the pH was raised to unfavorable conditions and new AFM images were taken to check whether the NPs were still adhering. During these measurements the systems were never dried. Similar tests were carried out with Sample B and C NPs.

The bare NP and binary systems were studied by TEM. TEM Images were obtained on an image-corrected FEI Titan 80–300 microscope operated at 300 kV, equipped with a Gatan Tridiem energy filter providing an information limit of 0.08 nm in TEM mode. HAADF-STEM operation with a nominal probe size of 0.19 nm was performed by diluting the material in MilliQ water and dispersing it on a carbon-coated Au grid (Quantifoil GmbH, Großlobichau, Germany).

3. Results and Discussion

3.1. Determination of Zeta-Potentials of Flat Collector Surfaces Covered by POMs

Figure 1 shows the results of experiments with different MeAl_{12}^{n+} specimen in contact with flat sapphire-c and fused SiO_2 crystals exposing overall 4 cm^2 collector surface area. In MeAl_{12}^{n+} , Me can be Al and Ga ($n = 7$) or Ge ($n = 8$). The charge of the Keggin-ions is pH-dependent, as shown in Scheme 2 [32,33,40]. The aqueous equilibria responsible for the behavior sketched in Scheme 2 may change in an unknown manner when the Keggin-ions are adsorbing to a surface.

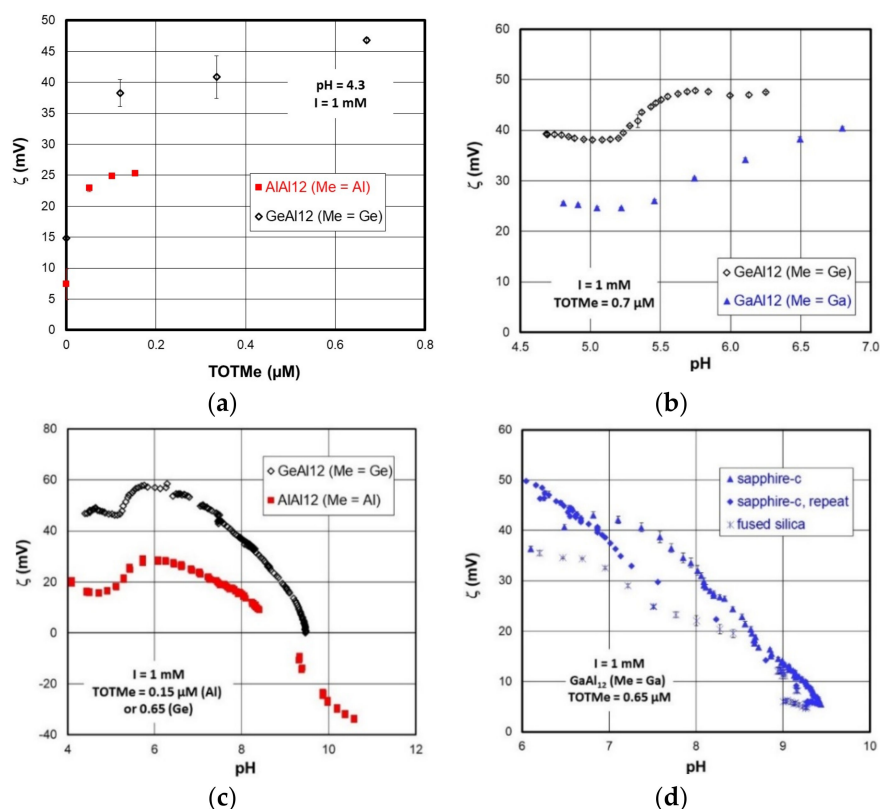


Figure 1. Zeta-potential of sapphire-c (a–d) or fused SiO_2 (d) in the presence of Keggin-ions in 1 mM ionic strength (NaCl). (a) Adsorption on sapphire-c at constant pH as a function of Keggin-ion concentration. (b) Behavior as a function of pH for constant Keggin-ion concentration for two different Keggin-ions. (c) Effect of pH for two different Keggin-ions at two different Keggin-ion concentrations. (d) Comparison of pH dependent behavior between sapphire-c and fused SiO_2 at constant GaAl_{12} -ion concentration. TOTMe represents the concentration of the central ion and thus to that of the Keggin-ion.

Figure 1a shows a comparison between Al_{13}^{7+} and GeAl_{12}^{8+} solutions for 1 mM NaCl solution at pH 4.3. The IEP of the collector surface is at about 4.5 [72]. The data reveal that the POMs adsorb on the initially positively charged collector surface ($\zeta \approx +10 \text{ mV}$ at pH 4.3). The presence of about $0.05 \mu\text{M}$ Al_{13}^{7+} is sufficient to increase zeta-potential by as much as 15 mV, and the effect of GeAl_{12}^{8+} is even more pronounced, i.e., the observed response is highly sensitive to the increase in charge of the adsorbing entity. This is confirmed in a pH-scan of sapphire-c zeta-potentials (Figure 1b) in the presence of about $0.7 \mu\text{M}$ GeAl_{12}^{8+} and GaAl_{12}^{7+} , respectively. A pronounced but unexpected pH dependence occurs at pH about 5.3 to 5.5, maybe due to the decomposition of the POM and subsequent adsorption on the collector surface of the species or resulting from decomposition or additional adsorption of previously dissolved Keggin-ions following the typical pH dependence of cation adsorption. In the present work, no attempt was made to study this phenomenon in more detail.

Figure 1c shows a more extended pH range in the results for Ge from Figure 1b ($0.17 \mu\text{M}$) and the results of an experiment in the presence of Al_{13} ($0.65 \mu\text{M}$). The IEPs obtained for both systems are at pH ≈ 9 . The unaggregated Keggin-ions in solution exhibit a very steep deprotonation at pH about 6.5 (Ga and Al), or 6.0 (Ge), see Scheme 2b. In this pH range, the point of zero charge should occur, but the IEP due to “adsorbed” Keggin-ions (or the products of the Keggin-ions) is much higher, i.e., in the typical range of aluminum oxide or hydroxide particles or aluminum hydroxide layers on sapphire-c [73].

Figure 1b,c shows a somewhat unconventional behavior in the sense that the zeta-potential increases with increasing pH. We are confident that this is due to the properties of the Keggin-ions. In fact, unpublished uptake data for GaAl_{12} on gibbsite show the same step-behavior that is seen on the

two figures, while the uptake on gibbsite from a Ga(III) solution of similar concentration (in Me) does not show this step (but was at 100 % for all pH values). Additionally, in these adsorption experiments, the Ga uptake in both cases was never zero at the lowest pH value studied (pH 4), but showed a constant value for GaAl₁₂ (around 80 %) before jumping to 100% at about pH 5.5 (i.e., in the range where the step in zeta-potential was observed in Figure 1b,c).

Figure 1d finally shows a comparison for the Ga compound on two different collector surfaces (sapphire-c and fused SiO₂). Results of interaction experiments with fused SiO₂ as a collector surface suggest that both surfaces are equally responsive to the Keggin-ions and could be used as collectors in applications devoted to other polymeric species (e.g., of radionuclides). The use of the less expensive fused SiO₂ is preferable, since the single crystals can hardly be reused without significant treatment due to the potentially irreversible interaction with many inorganic pollutants. The experiment with sapphire-c was reiterated by readjusting the pH at the end of the first experiment to acidic values, whereupon the upward pH-scan was started again. The data for the first titration on sapphire-c in the presence of GaAl₁₂ agree with those in Figure 1c for the other Keggin-ions on this collector surface. The higher concentration of Me in the case of Ga compared to Al results in a higher magnitude of the zeta-potential, while for similar concentrations the higher charge of the Ge compound again yielded higher zeta-potentials relative to the Ga case. In the experiments with Ge, at the high pH values strong buffering was observed, comparable to the behavior of GeAl₁₂ (Figure 1c) at similar Keggin-ion concentrations, with a steep decrease in zeta-potential close to the IEP. Under these conditions a pH increase was difficult to achieve, and in the case of the GaAl₁₂, the pH even decreased on adding base. For Al₁₃ no such buffering was observed, potentially due to the more than 4 times lower concentration. The observed buffering also occurs in titrations of the dissolved Keggin-ions (absence of a collector surface) at pH ≈ 6 for GeAl₁₂ and pH ≈ 6.5 for GaAl₁₂ and Al₁₃ depending on the total concentration (see Scheme 2b).

The reiteration experiment (Figure 1d) clearly shows at low pH the behavior has become different in the second pH-scan, whereas the behavior at pH > 8.5 is rather generic and does not depend on the nature of the collector surface. The buffering behavior and the difference in behavior at low pH for the two sapphire-c experiments support the idea that the Keggin-ions at pH > 9 have undergone irreversible changes (decomposition/aggregation or transformation). Thus, in the second run, the behavior changed probably due to the decomposition of the compounds at the high pH in the first run (at the latest). The behavior of the Keggin-ions on surfaces remains largely unexplored.

As a conclusion of the POM study, it appears that with the collector surfaces used here, small concentrations of polymeric units in a solution will be observable via the streaming current technique (if interaction occurs and if this interaction affects the charging properties of the collector surfaces, which is generally expected). In the case of extremely small sample volumes, it would be possible to deposit the sample on the collector surface, and then start the experiment with the usual 500 mL solution volume, assuming the interaction is similarly strong. In such a procedure, the analysis of the collector surfaces ideally before the streaming current measurements (to avoid possible leaching) and post-mortem would allow more detailed, ideally structural investigations.

3.2. Determination of Zeta-Potentials via Streaming Current Measurements on Quartz (001) Single Crystals in the Presence of Aqueous Sample A TiO₂ NPs

In the first part of this section, the results from separate size measurements of the TiO₂ Sample A NPs are reported. Subsequently, the charging properties of the involved surfaces are discussed, and finally, in some detail, the results of streaming current measurements at flat surfaces on the binary systems.

3.2.1. TiO₂ Sample A Size Measurements

Size measurements using the Brookhaven set-up indicated the presence of the expected sub 10 nm size NPs in the case of Sample A, along with larger aggregated NPs. AFM images of Sample A

suspensions deposited on a mica sheet from the stock suspension showed the primary NPs and no larger aggregates. The height distribution of the deposited NPs suggests a consistent size below 5 nm in this dimension. The lateral dimensions of aggregated particles are much larger than hydrodynamic radii obtained from the Brookhaven set-up and as subsequently confirmed by TEM.

The observation that primary NPs and larger aggregates coexist is not unusual, and has been reported, for example, for ferrihydrite. The primary NPs of this iron hydroxide are also in the sub 10 nm range, but the suspended material consists at least partly of larger agglomerates in aqueous media [74].

3.2.2. TiO₂ Sample A Charging Characteristics

Figure 2 shows zeta-potentials for Sample A NPs in 1 mM and 10 mM NaNO₃. The IEP of this sample is between pH 4.4 and 5.1 when the range of experimental data points with both positive and negative mobilities for the two salt media is considered. The ionic strength dependence of Sample A particle zeta-potentials is as expected (Figure 2), i.e., lower absolute values for higher ionic strength. The data at lower ionic strength will be used for comparison with the results of zeta-potential measurements discussed in the next section.

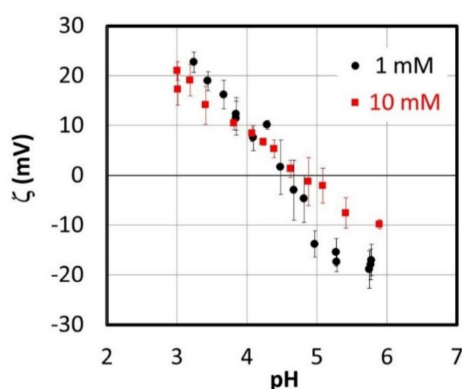


Figure 2. Zeta-potentials of Sample A NPs in 1 mM and 10 mM sodium nitrate solution.

Zeta-potential results for the flat collector surface, quartz (001), before and after addition of the NPs are shown in Figure 3a. The bare quartz (001) plane exhibits negative zeta-potentials for the pH values studied so that the IEP of the bare quartz (001) surface is below pH 4. Its precise value was not determined in the present study. The charging behavior of this plane is rather in agreement with the full red triangles than with the classical (Bolt-type) SiO₂ behavior (open triangles) in Scheme 2a.

The addition of TiO₂ NPs strongly affects the electrokinetic properties of the system, which is most evident from the observed charge reversal. The measured negative zeta-potential in the absence of NPs changes to slightly positive values in their presence below 4.6. This can only be caused by the adhesion of NPs to the quartz (001) plane. Since the charging of the two surfaces is pH dependent, the net interaction is a complex function of the individual charging behaviors. These are controlled by the relevant surface chemical reactions (equilibria), and the concomitant effects of interfacial potentials [26]. We cannot know the number of NPs on the collector surface, and only control the total amount of NPs in the present work. It is obvious though that, ultimately, the NPs govern the overall measured zeta-potential. The IEP of the “composite” system is at about pH 5.0, which corresponds to the IEP independently found for the pure NP system (Figure 2). Figure 3b directly compares the zeta-potentials of the bare NPs with those of the binary system (i.e., collector surface in presence of the NPs). The independent results are in surprisingly good agreement, which leads us to propose that streaming current measurements at flat surfaces could be a rather convenient way to determine the zeta-potential of NPs that are for some reason not accessible to conventional scattering methods. Such reasons could be limited amount of material, or difficulties due to very small size (see Section 3.1). Indeed, adhesion methods have been previously shown to yield reliable values for IEPs in comparable

systems, where large particles were used as collector surfaces [47]. The latter technique involves higher surface area, which makes it less sensible for small amounts of target material.

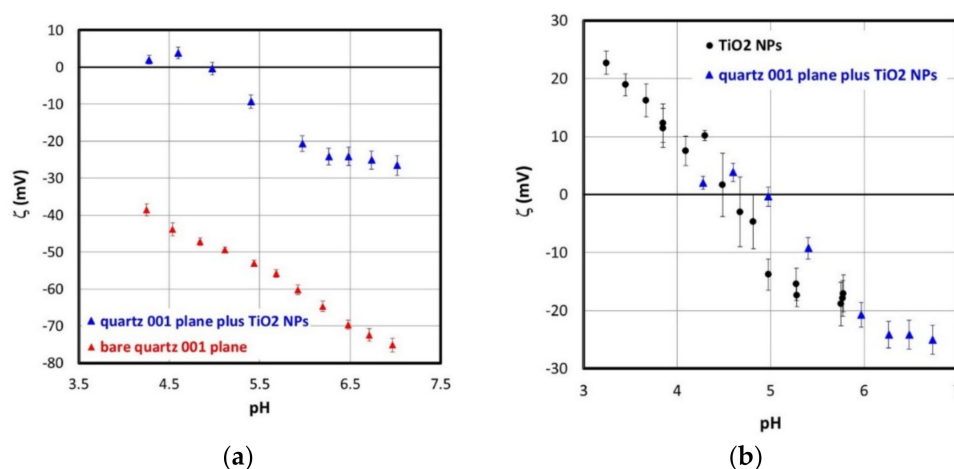


Figure 3. (a) Zeta-potential of the quartz (001) plane in the absence and presence of Sample A TiO₂ NPs (total amount 0.125 mg/m²). Background electrolyte is 1 mM NaNO₃; 0.5 mL of 1 g/L NP suspension was added to 500 mL of 1 mM NaNO₃ solution at pH around 4. (b) Comparison of the zeta-potentials in 1 mM NaNO₃ obtained for the colloidal system from electrophoretic mobilities and those obtained in the quartz (001)—TiO₂ system using zeta-potential from streaming current measurements at flat surfaces.

The comparison in Figure 3b further suggests that quartz (or more generally SiO₂) surfaces would, as in the case of the POMs, be good “test” (collector) surfaces. We propose that the determination of zeta-potentials from streaming current measurements at flat surfaces could allow the determination of the IEP of NPs, and we emphasize that only very small quantities are required for the measurements. A drawback arising from the injection of the TiO₂ NPs into the SurPass apparatus was contamination of the set-up. The NPs clearly remained in the closed cycle of the set-up, in particular on the surfaces of the glass cylinders that serve as syringes which press the solution through the flow-channel (Scheme 3). In subsequent measurements with various other surfaces, the results were still affected due to the persistence of TiO₂ NPs in the set-up. This entailed substantial cleaning efforts, and eventually required replacement of some parts (such as the glass cylinders), before standard results could be reproduced with the Anton Paar standard foil, Teflon [75], or sapphire-c [68] surfaces. We did not notice a general risk of such expensive contamination. For example, no persistent contamination was observed when POMs or SiO₂ NPs were injected to study their interaction with single crystal collectors. Additionally, the SiO₂ NPs used in the experiments discussed in a subsequent section were rapidly removed from the set-up and standard results were obtained after applying the usual cleaning procedures as was the case with the Keggin-ions.

Interestingly, the results in Figure 3 imply that NP retention on the substrate occurs even for unfavorable conditions ($\zeta_{\text{collector}} < -70$ mV, $\zeta_{\text{NP}} < -25$ mV), i.e., the data in Figure 3b suggest that the NPs adhere to the flat surface even when both individual surfaces bear negative charges. This was further verified by AFM measurements (Figure 4) on the sample retrieved from the set-up in contact with a solution at pH 7. A classical interaction model would suggest the NPs to be released under conditions, where both surfaces have a significant negative charge. However, the AFM measurements show that the NPs indeed persist on the quartz surface at the end of the experiment. This is not an artifact of drying. The samples were taken from the set-up after the emptying step (as controlled by the SurPass software, i.e., no unnecessary rinse) and were then dismantled from the holders. Lack of reversibility has also been reported in Quartz Crystal Microbalance (QCM) experiments for TiO₂ NP interaction with SiO₂ as a flat collector surface [76]. Only at very high pH (pH 9) or if the NPs had been deposited at the high pH, release of the NPs could be observed in that study [76]. The fact

that adhesion occurred when negatively charged TiO_2 NPs were contacted with negatively charged SiO_2 collector surfaces seems to be rather the rule than the exception as it was also found in direct adhesion experiments [23]. From the AFM investigation we can also discuss the particle size of the NPs on the collector surface. The height of the major part of the NPs is clearly below 10 nm, while lateral dimensions are between 80 and 100 nm (Figure 4d), c.f. Section 3.2.1.

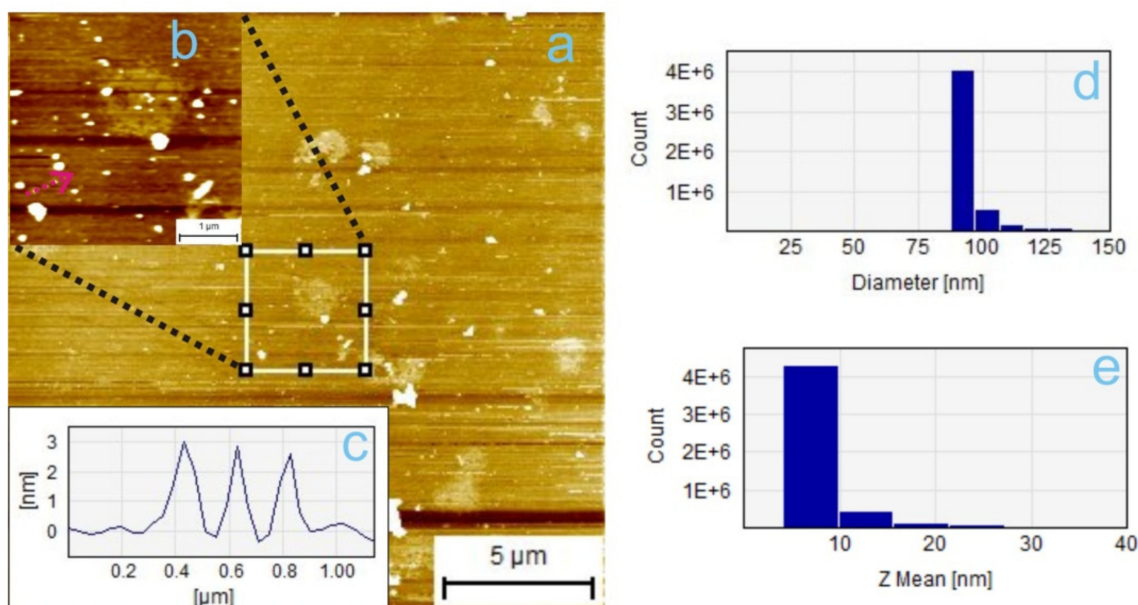


Figure 4. (a) AFM images of the quartz (001) surface after the zeta-potential measurements in the presence of the NPs Sample A (Figure 3, blue data points, pH 7); (b) magnified image of nanoparticles on surface; (c) height profile (along the line highlighted in b of NPs; (d,e) mean diameter and mean height of the NPs.

In summary, as for the POM systems the results from streaming current measurements at flat surfaces yield reliable data on the properties of the added NPs. Interestingly, interaction of NPs with collector surfaces also occurred under “unfavorable” conditions and was irreversible. This latter aspect also reported in independent studies is further addressed in a subsequent section.

3.3. Interaction of Sample A TiO_2 Nanoparticles with SiO_2 Collector Particles

The experiments leading to the data presented in Figure 3 were performed at a given ratio between the mass of NPs and the quartz collector surface area. The results suggest that streaming current measurements at flat surfaces yield the IEP of the NPs. It is important to verify that the charge of the collector (SiO_2) surface is not significantly affecting the results. Or in other words, it should be verified that the target particle surface coverage on the collector surface is sufficient to dominate the measured zeta-potentials. Binary particle suspensions (Sample A TiO_2 NPs in the presence of excess Aerosil OX 50 NPs substantially larger in size than the Sample A primary NPs) were studied by combined electrokinetic and TEM/AFM approaches.

The bare SiO_2 NPs in 1 mM NaNO_3 exhibit an IEP at pH 1 (Figure 5a). The ionic strength necessarily changes at such low pH, which will affect the magnitude of the electrokinetic data, but will ideally not change the sign. Figure 5a also includes mobilities measured for Sample A TiO_2 NPs and we obtain an IEP in the range measured independently (see Figure 1).

Based on Figure 5a, the SiO_2 colloids bear a negative electrokinetic charge over the whole pH range of interest (as do the flat SiO_2 collectors). Within the currently studied pH-range, conditions for hetero-aggregation should be favorable for $\text{pH} < 5$ at the latest, and be most unfavorable at around pH 8.

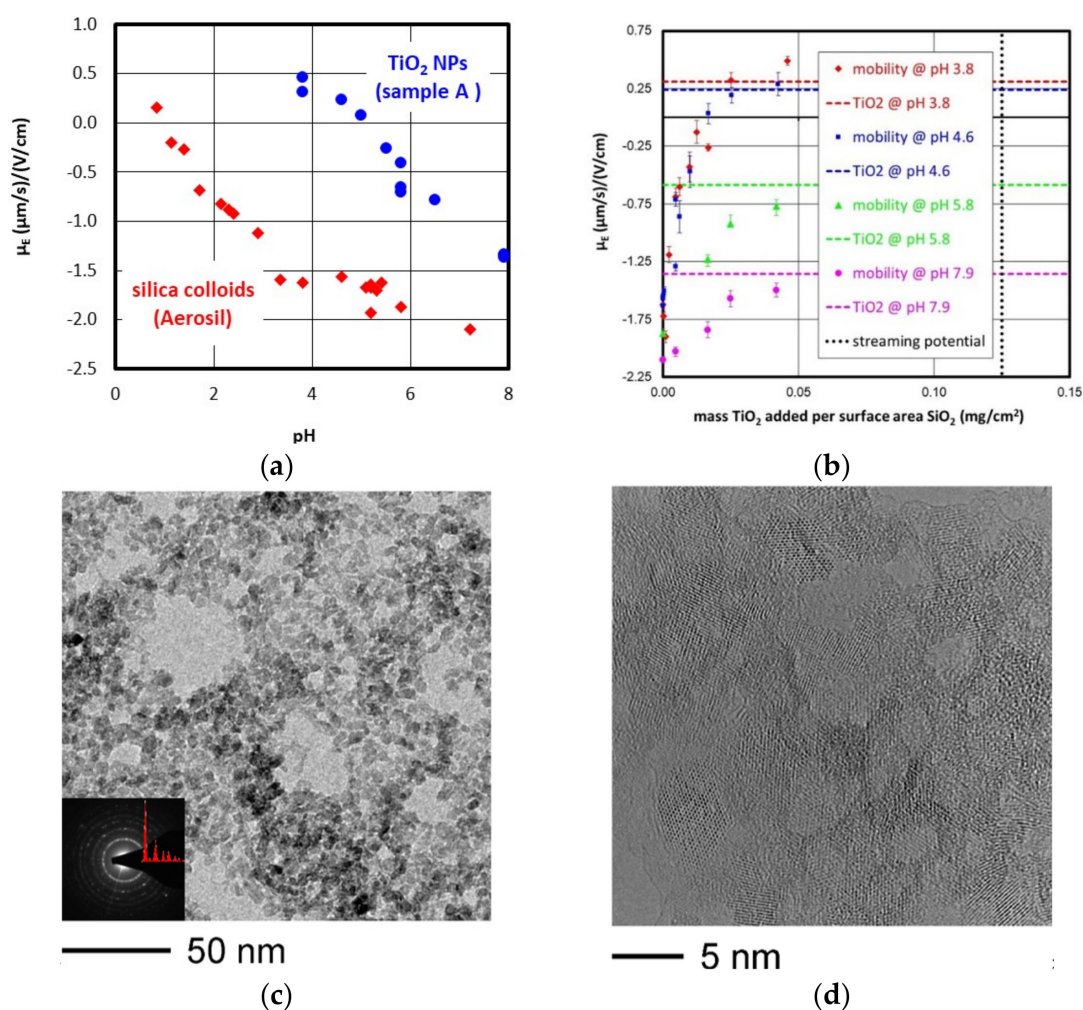


Figure 5. (a) Electrophoretic mobility of SiO_2 (AEROSIL OX 50) nanoparticles and TiO_2 NPs (Sample A) in the absence of the respective other sample as a function of pH in nominal 1 mM NaNO_3 electrolyte. (b) Electrophoretic mobility of AEROSIL OX 50 nanoparticles in the presence of TiO_2 NPs (Sample A) at selected pH values (represented by different colors) in 1 mM NaNO_3 electrolyte. The dashed horizontal lines correspond to the mobility values measured for bare Sample A TiO_2 NPs (in the absence of SiO_2) at the respective pH (indicated by the color). The vertical line corresponds to the condition under which the zeta-potential experiments with quartz (001) and Sample A were carried out. (c) Bright-field TEM overview image of Sample A TiO_2 NPs with an SAED pattern as inset. (d) HRTEM micrograph of the Sample A TiO_2 NPs.

Figure 5b shows measured mobilities of binary suspensions with various ratios of Sample A TiO_2 mass relative to the available SiO_2 surface area as measured for different pH values. The line perpendicular to the x -axis at about $0.125 \text{ mg}/\text{cm}^2$ corresponds to the condition in the streaming current measurements shown in Figure 3b. The horizontal dashed lines correspond to the results obtained for the bare TiO_2 NPs. Figure 5b clearly shows that the mobilities of the binary systems approach those of the pure TiO_2 NP system with increasing TiO_2 NP content. Thus, for the condition concerning the streaming current measurement at the flat surface the overall charging properties of the system should indeed have been controlled by the NPs. Interestingly, the trends of the electrophoretic mobility at all pH values studied, i.e., for positive, neutral and negative NPs on the negatively charged SiO_2 NPs, corroborate attractive interactions under “unfavorable” conditions. This would mean that the interaction between the NPs and the SiO_2 surfaces is beyond simple electrostatic attractions and could even overcome electrostatic repulsion. This concurs with the zeta-potential data from the previous

section, and with the observation that (after the experimental period with the SurPass) the NPs stuck so strongly to the glass syringes that the latter had to be replaced before standard results could be reproduced with the SurPass.

Our results agree with work by others [77] showing that with sufficient TiO_2 , the composite system loses the SiO_2 properties and assumes those of the TiO_2 NPs. In the cited work, several SiO_2 supports (particles varying in size) were tested and the observed interaction occurred both with near-neutral SiO_2 and positively charged TiO_2 and when the system was exposed to pH values above the IEP of TiO_2 . Furthermore, the trend of increasing IEP with increasing amounts of TiO_2 was retrieved [77,78]. Interaction of small TiO_2 NPs with larger grains of quartz was also reported to occur from pH 3 to 8, i.e., even under unfavorable conditions [23]. The above mentioned QCM data [76] and the isotherm data clearly agree with our results.

Obviously, and in particular for the unfavorable conditions, the mobility data are only meaningful if the added NPs indeed adhered to the bigger SiO_2 particles, i.e., there should be no significant separate contribution to the observed electrophoretic mobility from free TiO_2 NPs. Although the independent data cited above support this, we verified by TEM whether the TiO_2 Sample A NPs adhered to the SiO_2 NPs. We first discuss the results for bare NPs of Sample A and the SiO_2 NPs.

The bright field TEM image with an inset of the selected area electron diffraction pattern (SAED) and HRTEM micrograph of the bare NPs are shown in Figure 5c,d, respectively. The measured d-spacing from the SAED pattern and from the fast Fourier transformation of the HRTEM micrograph are consistent with the PXRD results of dried TiO_2 (data not shown).

Figure 6a,b indicates that no aggregation of the NPs in the stock suspension over time has occurred, so that observed aggregation on a collector surface (Figure 4b) is not due to the instability of the NPs in the stock suspension. Since the injection of the NPs was done at low pH, it cannot be inferred whether aggregates at the surface formed at the low pH or only with increasing pH. Concerning the collector surfaces relevant to the data in Figure 5a,b and Figure 6c shows that the bare SiO_2 NPs are aggregates of smaller primary NPs.

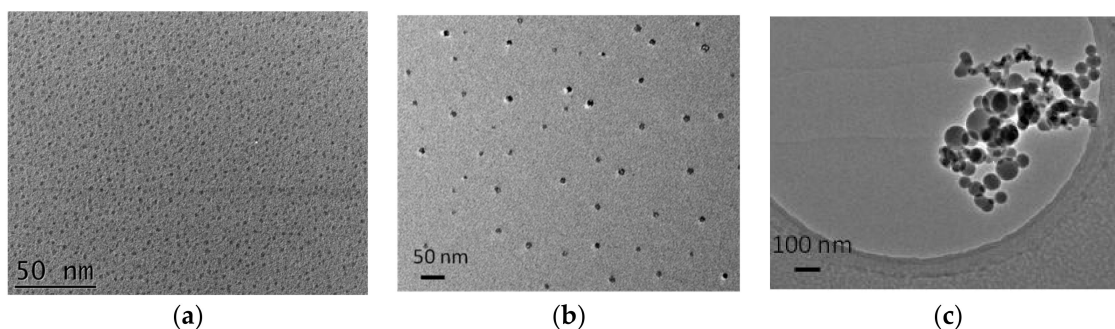


Figure 6. Bright field TEM images of Sample A TiO_2 NPs (a) directly after synthesis and (b) after the end of the experiment period, and (c) of the SiO_2 .

With respect to the macroscopic data, the electrokinetic method could easily lead to misinterpretation, and therefore we have attempted to prove the presence of the NPs on the SiO_2 NPs and show here the results for the most unfavorable conditions investigated (Figure 7). At pH = 8, the mobility of the two kinds of NPs is showing strongly negative values.

Figure 7 exhibits evidence for the association of the TiO_2 Sample A NPs with the SiO_2 colloids. Here, high-angle annular dark field–scanning transmission electron microscopy (HAADF-STEM) with EDX area scans clearly show the fingerprint of TiO_2 NPs on the SiO_2 colloid for the samples after the addition at pH 8 (i.e., under unfavorable conditions).

From the experimental data, we can conclude that the small NPs are attracted to the collector surfaces (the SiO_2 type flat plates or the SiO_2 aggregates) and finally control the electrokinetic properties of the system.

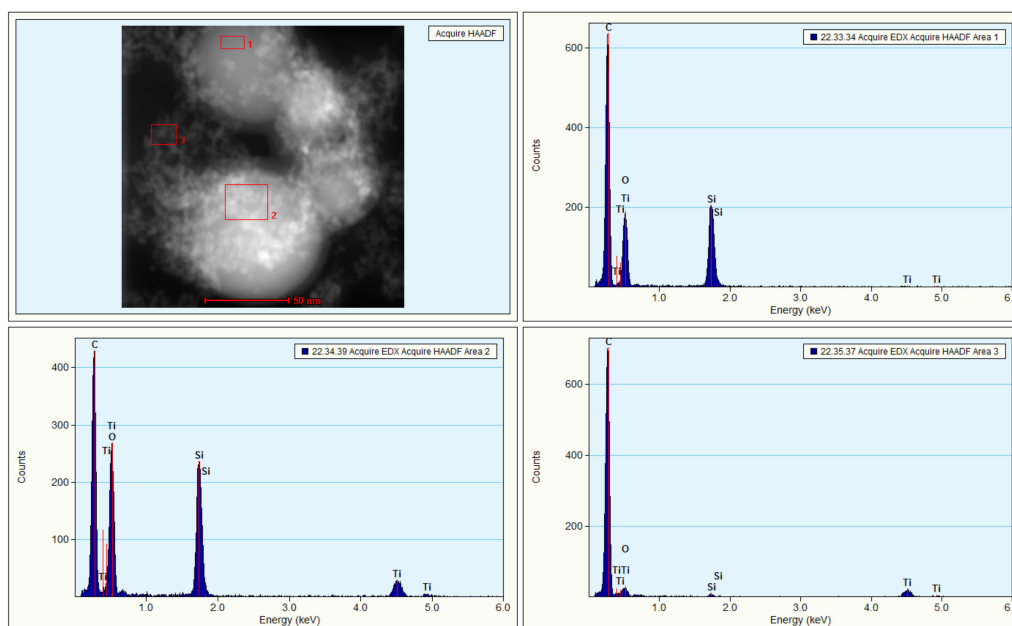


Figure 7. STEM-EDX area scans of Sample A TiO_2 -NP/ SiO_2 -colloid agglomerates at pH 8. The three areas marked in red of the area scans depict (1) Si and O, (2) Ti and O and (3) Si, Ti and O signals respectively.

3.4. Additional Binary Systems Involving SiO_2 and TiO_2 Surfaces

In this section, we report the results of further experiments focused on interactions between SiO_2 and TiO_2 surfaces under “unfavorable” conditions. We first present the charging properties and then discuss the results of the interaction studies.

3.4.1. Particle Charging Characteristics of TiO_2 NPs (Samples B and C)

The zeta-potentials of TiO_2 NP Samples B and C are shown in Figure 8a,b. Sample B NPs have their IEP at about pH 6 (Figure 8a), i.e., slightly higher than Sample A (Figure 2). Compared to Samples A and B, TiO_2 nanowires (Sample C) exhibit a significantly lower IEP at pH 3.5 (Figure 8b). The data for Sample C are in agreement with independent electrokinetic measurements on this material [63]. Thus, concerning interactions with SiO_2 type systems, for Samples B and C, clearly favorable pH ranges for adhesion with negative SiO_2 NPs (i.e., the range of pH values studied here for the mixed systems) and positive TiO_2 NPs (i.e., pH < 6, and pH < 3.5 for Samples B and C, respectively) can be defined. Based on the IEPs of the different materials alone, the very small “spherical” NPs (Samples A and B) would exhibit a broader pH-range of “favorable” conditions compared to Sample C.

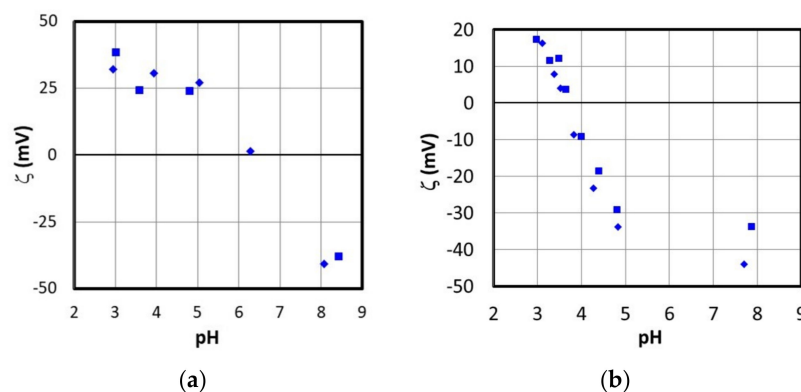


Figure 8. Zeta-potentials of TiO_2 NPs (Samples B and C) and in 1 mM NaNO_3 solutions. (a) TiO_2 Sample B. (b) TiO_2 Sample C.

3.4.2. Sample B NP Interaction with Quartz Collector Surfaces

The interaction of Sample B (positively charged, charge-stabilized at low pH in the stock suspension) TiO_2 NPs with negatively charged surfaces was similar to the results with Sample A. Compared to Sample A, Sample B NPs have similar sizes and slightly higher IEP (Figure 5b). The AFM interaction study showed that Sample B NPs adhere to negatively charged quartz (001) under all conditions tested, i.e., irrespective of the pH and even if both surface charges were negative. Furthermore, Sample B NPs could not be released by switching the conditions from “favorable” to “unfavorable”.

3.4.3. Sample C NPs in the Presence of Quartz Collector Surfaces

To study morphologically different NPs Sample C (TiO_2 NWs) was contacted with flat negative quartz (001) collector surfaces. Sample C NPs not only have a different morphology compared to Samples A and B. They are also larger in at least one dimension, and the IEP of Sample C (Figure 5c) is significantly lower than for Samples A and B, leading to “unfavorable” conditions for $\text{pH} > 3.5$. Unlike for Samples A and B, AFM showed that Sample C NPs only adhered to the test surfaces under favorable conditions, i.e., $\text{pH} < 3.5$. However, once adhering to the supporting surfaces, they were not released under unfavorable conditions. This is different from the results of Fattison et al. [76] who did observe release. However, they observed this only at $\text{pH} 9$.

3.5. Interactions of SiO_2 Nanoparticles with Flat Rutile Collector Surfaces

This system was studied to further verify the ability of streaming current measurements at flat surfaces to retrieve the properties of NPs. Experiments were carried out at about $\text{pH} 4$ in 1 mM KCl solutions. The Ludox TMA NPs were initially investigated by conventional electrophoretic mobility, resulting in zeta-potentials of about -20 mV between $\text{pH} 3.5$ and 4.5 .

The IEP of the rutile (001) plane was found to be at pH about 5.9 in 1 mM KCl and 1 mM NaClO_4 (data not shown). This is in agreement with independent AFM force distance measurements, suggesting an IEP between 5.5 and 5.8 [79]. The single crystal collector surface involved in this experiment could be a good candidate to study negatively charged NPs.

Figure 9 shows that with increasing concentration of the SiO_2 NPs, the initially positive rutile surface turns negative (at about 2 mg/cm^2 SiO_2 concentration) and asymptotically attains the zeta-potential of the SiO_2 NPs. As in the inverse system, the streaming current measurements at flat surfaces make it possible (i) to obtain the sign of the charge of the NPs at very low NP concentration, and (ii) to retrieve good estimates of the NP zeta-potential at sufficiently high NP concentration.

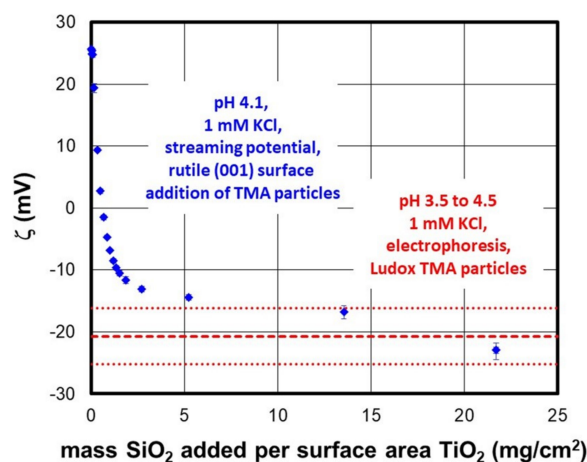


Figure 9. Zeta-potential of rutile (001) single crystals at $\text{pH} 4.1$, in 1 mM KCl, as a function of Ludox TMA solid concentration (blue symbols) and average zeta-potential of Ludox TMA nanoparticles (dotted line). The fine dotted lines show the three sigma limits of the repeated measurements on the nanoparticles.

The IEP of the combined system at the end of the addition experiment was below pH 4 (as inferred from Figure 9). The sample involving SiO₂ NPs attached to the rutile (001) planes was exposed to high pH (where both surfaces are negatively charged, i.e., “unfavorable” conditions) by carrying out a pH scan. The solution was then replaced by a SiO₂ free 1 mM KCl solution of pH 4 and another pH scan was carried out. It was observed that the IEP occurred at pH 5.1 (compared to 5.9 prior to contact with SiO₂ NPs) for the collector surface, i.e., rutile (001), suggesting detachment of a large part but not all of the SiO₂ NPs under “unfavorable” conditions. While the strong interactions in this system where we inversed the target NP and collector role were again established, reversibility again showed new nuances, in the sense that part of the NPs could be released under high pH conditions, even if they were attached at low pH conditions.

4. Conclusions and Summary

Various aspects of using streaming current measurements at flat surfaces as a tool for studying the properties of POMs and NPs were addressed, and the results of our experimental work suggest the following:

- The proposed approach is able to detect and collect very small NPs present in very small quantities.
- The collected NPs can subsequently (i.e., after, e.g., a streaming current experiment) be used for further studies.
- The interfacial behavior can be studied in more detail addressing for example interactions or remobilization under what we defined as “unfavorable” conditions.

As a conclusion, zeta-potential determination of flat surfaces with known charging properties by streaming current measurements could be a simple and efficient way of obtaining reliable zeta-potentials for NPs that are not accessible by the more common measurements (either being too small and/or not available in sufficient amounts). Our zeta-potential data derived after NP addition to the collector surface are similar to zeta-potentials obtained for the bare NPs by conventional electrophoretic mobility measurements. The streaming current/potential technique requires sufficient coverage of the collector surface by the colloidal or nanosized particles. This was shown to be the case for the respective system via a comparison with separate results for the bare NPs. In the inverse system, where SiO₂ NPs were added to TiO₂ single crystals, the dependence on NP concentration was studied in more detail via streaming current measurements at flat surfaces. The results corroborate that very little material is required to obtain information about the sign of charge of the NPs (under favorable conditions). With sufficient addition, the properties of the NPs were also retrieved in this case.

We have furthermore shown that different TiO₂ NPs (Samples A, B and C) may exhibit very strong interactions with SiO₂ surfaces in aqueous solutions. The interactions of Sample A with SiO₂ type surfaces were found to be strong enough to overcome electrostatic repulsion. Both streaming current and electrokinetic data suggest that the NPs adhere to a negatively charged surface when they bear a negative charge themselves. Results from AFM and (S)TEM studies show more direct evidence for this. The fact that the TiO₂ NPs are so strongly retained on the SiO₂ support suggests that such purely inorganic NPs will not be mobile in natural environments, which might be different for NPs that are stabilized by some organic layer.

The interactions of polymeric radionuclide species with surfaces have been studied by synchrotron methods [80] without knowledge about the charging properties. Our results involving POMs suggest that charging properties of such polymeric species could be studied by measurements of zeta-potentials at flat surfaces. Polymeric species of Plutonium have been reported to be quite mobile in natural environment [56]. The study of their interaction with surfaces would be an important step in understanding this unexpected mobility. In several systems, polymeric or colloidal species of radionuclides have been identified in solubility studies, but neither their composition nor their physico-chemical properties are precisely known [81,82]. Investigations involving the procedure suggested here could shed some light on the IEP of such hazardous and potentially mobile species.

Once concentrated on a support the composition could be further studied. The success obviously depends on the (known) properties of the support and the (unknown) properties of the NPs, which requires trial and error or estimates based on available information.

The results that might suggest some effect of size (i.e., Sample C vs. Samples A and B) are in line with observations that at the very small sizes (i.e., around 10 nm), particle properties start to change. Thus, the charge density of NPs with identical properties but decreasing size start to be affected by particle geometry at these very small sizes [83]. Experiments and independent calculations also support the idea that small NPs exhibit higher surface charge densities [84]. Finally, size can even affect the point of zero charge as has been demonstrated for ultrafine maghemite NPs ($\gamma\text{-Fe}_2\text{O}_3$) in the size range from 12 to 7.5 to 3.5 nm, respectively [85]. According to the literature, particle–particle interactions between identical NPs of sufficiently small size exhibit non-additivity [35].

Hetero-aggregation under unfavorable conditions for various sizes of TiO_2 NPs with SiO_2 has been previously observed [23]. The interaction of the two kinds of NPs has led to the appearance of new infrared bands [22], which would suggest forces beyond those resulting from barely physical interactions controlled by charge. This is in agreement with our results under “unfavorable” conditions.

The potential effect of aging on the measured zeta-potentials or electrophoretic mobilities is beyond the scope of the present study. Since we concluded, in agreement with previous reports, that there might be chemical interactions between SiO_2 and TiO_2 samples, it is likely that such interactions affect the behavior of the binary suspension significantly, for example, due to the dissolution of SiO_2 and the adsorption of dissolved silicic acid on TiO_2 . Aging certainly plays a role in the POM systems, which was obvious in some of the experimental data.

Author Contributions: J.L. carried out the sample treatment and electrokinetic experiments. G.K.D. carried out the AFM experiments. V.S.K.C. carried out the TEM experiments. E.R., A.S. and L.V. carried out the NP synthesis. All authors contributed to the experimental design, interpretation of data and writing of the manuscript. All authors have read and agreed to the published version of the manuscript.

Funding: G.K.D. was supported by the Helmholtz Program NUSAFE. The work has received partial funding by the Federal Ministry of Economics and Technology (BMWi) under the joint KIT-INE, GRS research projects “KOLLORADO-e2” (02E11456A) and the European 7th Framework Program (FP7/2007-2011) under grant agreement no. 295487 (BELBaR Project) and Ramanujan Fellowship (SB/S2/RJN-006/2016) and ECR project (ECR/2017/000707) from DST, India. E.R. thanks KIT and CMM for sustainable research funding.

Acknowledgments: We acknowledge support by the KIT-Publication Fund of the Karlsruhe Institute of Technology. E.R. thanks KNMF (Karlsruhe Nano Micro Facility) for SAED and HR-TEM measurements.

Conflicts of Interest: The authors declare no conflict of interest.

References and Notes

- Nowack, B.; Ranville, J.F.; Diamond, S.; Gallego-Urrea, J.A.; Metcalfe, C.; Rose, J.; Horne, N.; Koelmans, A.A.; Klaine, S.J. Potential scenarios for nanomaterial release and subsequent alteration in the environment. *Environ. Toxicol. Chem.* **2012**, *31*, 50–59. [[CrossRef](#)] [[PubMed](#)]
- Nowack, B. The behavior and effects of nanoparticles in the environment. *Environ. Pollut.* **2009**, *157*, 1063–1064. [[CrossRef](#)]
- Nowack, B.; Bucheli, T.D. Occurrence, behavior and effects of nanoparticles in the environment. *Environ. Pollut.* **2007**, *150*, 5–22. [[CrossRef](#)] [[PubMed](#)]
- Slomberg, D.L.; Schoenfisch, M.H. Silica Nanoparticle Phytotoxicity to *Arabidopsis thaliana*. *Environ. Sci. Technol.* **2012**, *46*, 10247–10254. [[PubMed](#)]
- Miralles, P.; Church, T.L.; Harris, A.T. Toxicity, Uptake, and Translocation of Engineered Nanomaterials in Vascular plants. *Environ. Sci. Technol.* **2012**, *46*, 9224–9239. [[CrossRef](#)] [[PubMed](#)]
- Barton, L.E.; Auffan, M.; Durenkamp, M.; McGrath, S.; Bottero, J.-Y.; Wiesner, M.R. Monte Carlo simulations of the transformation and removal of Ag, TiO_2 , and ZnO nanoparticles in wastewater treatment and land application of biosolids. *Sci. Total Environ.* **2015**, *511*, 535–543. [[CrossRef](#)]

7. Schaumann, G.E.; Philippe, A.; Bundschuh, M.; Metreveli, G.; Klitzke, S.; Rakcheev, D.; Grün, A.; Kumahor, S.K.; Kühn, M.; Baumann, T.; et al. Understanding the fate and biological effects of Ag- and TiO₂-nanoparticles in the environment: The quest for advanced analytics and interdisciplinary concepts. *Sci. Total Environ.* **2015**, *535*, 3–19. [[CrossRef](#)]
8. Farkas, J.; Peter, H.; Gesielski, T.M.; Thomas, K.V.; Sommaruga, R.; Salvenmoser, W.; Weyhenmeyer, G.A.; Tranvik, L.J.; Jenssen, B.M. Impact of TiO₂ nanoparticles on freshwater bacteria from three Swedish lakes. *Sci. Total Environ.* **2015**, *535*, 85–93. [[CrossRef](#)]
9. Chen, L.; Sabatini, D.A.; Kibbey, T.C.G. Role of the Air–Water Interface in the Retention of TiO₂ Nanoparticles in Porous Media during Primary Drainage. *Environ. Sci. Technol.* **2008**, *42*, 1916–1921. [[CrossRef](#)]
10. Sun, J.; Guo, L.-H.; Zhang, H.; Zhao, L. UV Irradiation Induced Transformation of TiO₂ Nanoparticles in Water: Aggregation and Photoreactivity. *Environ. Sci. Technol.* **2014**, *48*, 11962–11968. [[CrossRef](#)]
11. Hu, J.; Shipley, H.J. Evaluation of desorption of Pb (II), Cu (II) and Zn (II) from titanium dioxide nanoparticles. *Sci. Total Environ.* **2012**, *431*, 209–220. [[CrossRef](#)] [[PubMed](#)]
12. Erhayem, M.; Sohn, M. Stability studies for titanium dioxide nanoparticles upon adsorption of Suwannee River humic and fulvic acids and natural organic matter. *Sci. Total Environ.* **2014**, *468*, 249–257. [[CrossRef](#)] [[PubMed](#)]
13. Maczka, E.; Luetzenkirchen, J.; Kosmulski, M. The significance of the solid-to-liquid ratio in the electrokinetic studies of the effect of ionic surfactants on mineral oxides. *J. Colloid Interface Sci.* **2013**, *393*, 228–233. [[CrossRef](#)] [[PubMed](#)]
14. Ju-Nam, Y.; Lead, J.R. Manufactured nanoparticles: An overview of their chemistry, interactions and potential environmental implications. *Sci. Total Environ.* **2008**, *400*, 396–414. [[PubMed](#)]
15. Petosa, A.R.; Jaisi, D.P.; Quevedo, I.R.; Elimelech, M.; Tufenkji, N. Aggregation and Deposition of Engineered Nanomaterials in Aquatic Environments: Role of Physicochemical Interactions. *Environ. Sci. Technol.* **2010**, *44*, 6532–6549. [[CrossRef](#)] [[PubMed](#)]
16. Goldberg, E.; Scheringr, M.; Bucheli, T.D.; Hungerbuhler, K. Critical Assessment of Models for Transport of Engineered Nanoparticles in Saturated Porous Media. *Environ. Sci. Technol.* **2014**, *48*, 12732–12741. [[CrossRef](#)]
17. Darbha, G.K.; Fischer, C.; Michler, A.; Luetzenkirchen, J.; Schäfer, T.; Heberling, F.; Schild, D. Deposition of Latex Colloids at Rough Mineral. Surfaces: An Analogue Study Using Nanopatterned Surfaces. *Langmuir* **2012**, *28*, 6606–6617. [[CrossRef](#)]
18. Martin Cabanas, B.; Lützenkirchen, J.; Leclercq, S.; Barboux, P.; Lefevre, G. Surface charging patterns of stainless alloys—Effect of ageing in conditions of primary cooling circuit of pressurized water reactors. *J. Nucl. Mater.* **2012**, *430*, 150–155. [[CrossRef](#)]
19. Li, K.; Chen, Y.; Zhang, W.; Pu, Z.; Jiang, L.; Chen, Y. Surface Interactions Affect the Toxicity of Engineered Metal. Oxide Nanoparticles toward Paramecium. *Chem. Res. Toxicol.* **2012**, *25*, 1675–1681. [[CrossRef](#)]
20. Florez, L.; Herrmann, C.; Cramer, J.M.; Hauser, C.P.; Koynov, K.; Landfester, K.; Crespy, D.; Mailänder, V. How Shape Influences Uptake: Interactions of Anisotropic Polymer Nanoparticles and Human Mesenchymal Stem Cells. *Small* **2012**, *8*, 2222–2230. [[CrossRef](#)]
21. Som, C.; Wick, P.; Krug, H.; Nowack, B. Environmental and health effects of nanomaterials in nanotextiles and facade coatings. *Environ. Int.* **2011**, *37*, 1131–1142. [[CrossRef](#)] [[PubMed](#)]
22. Güleriyüz, H.; Filiat, C.; Euvrard, M.; Buron, C.; Lakard, B. Novel strategy to prepare polyaniline—Modified SiO₂/TiO₂ composite particles. *Synth. Met.* **2013**, *181*, 104–109. [[CrossRef](#)]
23. Dietrich, L.A.; Sahu, M.; Biswas, P.; Fein, J.B. Experimental study of TiO₂ nanoparticle adhesion to silica and Fe(III) oxide-coated silica surfaces. *Chem. Geol.* **2012**, *332*, 148–156. [[CrossRef](#)]
24. Bahadur, J.; Sen, D.; Mazumder, S.; Sastry, P.U.; Paul, B.; Bhatt, H.; Singh, S.G. One-Step Fabrication of Thermally Stable TiO₂/SiO₂ Nanocomposite Microspheres by Evaporation-Induced Self-Assembly. *Langmuir* **2012**, *28*, 11343–11353. [[CrossRef](#)] [[PubMed](#)]
25. He, C.; Tian, B.; Zhang, J. Thermally stable SiO₂-doped mesoporous anatase TiO₂ with large surface area and excellent photocatalytic activity. *J. Colloid Interface Sci.* **2010**, *344*, 382–389. [[CrossRef](#)]
26. Lutzenkirchen, J.; Behra, P. A new approach for modelling potential effects in cation adsorption onto binary (hydr)oxides. *J. Contam. Hydrol.* **1997**, *26*, 257–268. [[CrossRef](#)]
27. De Faria, L.; Trasatti, S. Effect of composition on the point of zero charge of RuO₂ + TiO₂ mixed oxides. *J. Electroanal. Chem.* **1992**, *340*, 145–152. [[CrossRef](#)]

28. Reymond, J.; Kolenda, F. Estimation of the point of zero charge of simple and mixed oxides by mass titration. *Powder Technol.* **1999**, *103*, 30–36. [[CrossRef](#)]
29. Mustafa, S.; Dilara, B.; Nargis, K.; Naeem, A.; Shahida, P. Surface properties of the mixed oxides of iron and silica. *Colloids Surf. A Physicochem. Eng. Asp.* **2002**, *205*, 273–282. [[CrossRef](#)]
30. Schwarz, J.; Driscoll, C.; Bhanot, A. The zero point of charge of silica—Alumina oxide suspensions. *J. Colloid Interface Sci.* **1984**, *97*, 55–61. [[CrossRef](#)]
31. Koopal, L.K.; Dukhin, S.S. Modelling of the double layer and electrosorption of a patchwise heterogeneous surface on the basis off its homogeneous analogue 1. Non-interacting patches. *Colloids Surf. A Physicochem. Eng. Asp.* **1993**, *73*, 201–209. [[CrossRef](#)]
32. Furrer, G.; Ludwig, C.; Schindler, P.W. On the Chemistry of the Keggin Al₁₃ Polymer.1. Acid-Base Properties. *J. Colloid Interface Sci.* **1992**, *149*, 56–67. [[CrossRef](#)]
33. Lee, A.P.; Furrer, G.; Casey, W.H. On the acid-base chemistry of the Keggin polymers: GaAl₁₂ and GeAl₁₂. *J. Colloid Interface Sci.* **2002**, *250*, 269–270. [[CrossRef](#)] [[PubMed](#)]
34. Hernandez, J. Synthèse de Nanoparticules D'Oxydes de fer et D'Aluminium pour L'Étude de L'Adsorption D'Entités Inorganiques Polycondensées. Conséquences sur la Stabilisation des Dispersions. Ph.D. Thesis, Université Paris 6, Paris, France, 1998.
35. Batista, C.A.S.; Larson, R.G.; Kotov, N.A. Nonadditivity of nanoparticle interactions. *Science* **2015**, *350*, 1242477. [[CrossRef](#)] [[PubMed](#)]
36. Davis, J.A.; James, R.O.; Leckie, J.O. Surface ionization and complexation at the oxide/water interface: I. Computation of electrical double layer properties in simple electrolytes. *J. Colloid Interface Sci.* **1978**, *63*, 480–499. [[CrossRef](#)]
37. Yates, D.E.; Levine, S.; Healy, T.W. Site-binding model of the electrical double layer at the oxide/water interface. *J. Chem. Soc. Faraday Trans. 1 Phys. Chem. Condens. Phases* **1974**, *70*, 1807–1818. [[CrossRef](#)]
38. Darbha, G.K.; Fischer, C.; Luetzenkirchen, J.; Schäfer, T. Site-Specific Retention of Colloids at Rough Rock Surfaces. *Environ. Sci. Technol.* **2012**, *46*, 9378–9387. [[CrossRef](#)]
39. Casey, W.H. Large Aqueous Aluminum Hydroxide Molecules. *Chem. Rev.* **2006**, *106*, 1–16. [[CrossRef](#)]
40. Lützenkirchen, J.; Marsac, R.; Casey, W.H.; Furrer, G.; Kupcik, T.; Lindqvist-Reis, P. The Effect of Monovalent Electrolytes on the Deprotonation of MA₁₂ Keggin Ions. *Aquat. Geochem.* **2015**, *21*, 81–97, Erratum in **2015**, *21*, 555. [[CrossRef](#)]
41. Bouby, M.; Lützenkirchen, J.; Dardenne, K.; Preocanin, T.; Denecke, M.A.; Klenze, R.; Geckeis, H. Sorption of Eu(III) onto titanium dioxide: Measurements and modeling. *J. Colloid Interface Sci.* **2010**, *350*, 551–561. [[PubMed](#)]
42. Bolt, G.H. Determination of the Charge Density of Silica Sols. *J. Phys. Chem.* **1957**, *61*, 1166–1169. [[CrossRef](#)]
43. García, D.; Lützenkirchen, J.; Petrov, V.; Siebentritt, M.; Schild, D.; Lefèvre, G.; Rabung, T.; Altmaier, M.; Kalmykov, S.; Duro, L.; et al. Sorption of Eu(III) on quartz at high salt concentrations. *Colloids Surf. A Physicochem. Eng. Asp.* **2019**, *578*, 123610. [[CrossRef](#)]
44. Lutzenkirchen, J.; Preocanin, T.; Kovačević, D.; Tomišić, V.; Lövgren, L.; Kallay, N. Potentiometric Titrations as a Tool for Surface Charge Determination. *Croat. Chem. Acta* **2012**, *85*, 391–417. [[CrossRef](#)]
45. Delgado, A.V.; González-Caballero, F.; Hunter, R.J.; Koopal, L.K.; Lyklema, J. Measurement and interpretation of electrokinetic phenomena. *J. Colloid Interface Sci.* **2007**, *309*, 194–224.
46. Scales, P.J.; Grieser, F.; Healy, T.W.; White, L.R.; Chan, D.Y. Electrokinetics of the Silica Solution Interface—A Flat-Plate Streaming Potential Study. *Langmuir* **1992**, *8*, 965–974. [[CrossRef](#)]
47. Kallay, N.; Torbic, Z.; Golic, M.; Matijevic, E. Determination of the Isoelectric Points of Several Metals by an Adhesion Method. *J. Phys. Chem.* **1991**, *95*, 7028–7032. [[CrossRef](#)]
48. Lin, X.Y.; Farhi, E.; Arribart, H. Determination of the Isoelectric Point of Planar Oxide Surfaces by a Particle Adhesion Method. *J. Adhes.* **1995**, *51*, 181–189. [[CrossRef](#)]
49. Adamczyk, Z.; Nattich, M.; Wasilewska, M.; Zaucha, M. Colloid particle and protein deposition—Electrokinetic studies. *Adv. Colloid Interface Sci.* **2011**, *168*, 3–28. [[CrossRef](#)]
50. Adamczyk, Z.; Zaucha, M.; Zembala, M. Zeta Potential Mica Cover. By Colloid Part: A Streaming Potential Study. *Langmuir* **2010**, *26*, 9368–9377.
51. Nattich-Rak, M.; Adamczyk, Z.; Sadowska, M.; Morga, M.; Oćwieja, M. Hematite nanoparticle monolayers on mica: Characterization by colloid deposition. *Colloids Surf. A-Physicochem. Eng. Asp.* **2012**, *412*, 72–81. [[CrossRef](#)]

52. Tiede, K.; Hassellöv, M.; Breitbarth, E.; Chaudhry, Q.; Boxall, A.B. Considerations for environmental fate and ecotoxicity testing to support environmental risk assessments for engineered nanoparticles. *J. Chromatogr. A* **2009**, *1216*, 503–509. [[CrossRef](#)] [[PubMed](#)]
53. Klaine, S.J.; Alvarez, P.J.; Batley, G.E.; Fernandes, T.F.; Handy, R.D.; Lyon, D.Y.; Mahendra, S.; McLaughlin, M.J.; Lead, J.R. Nanomaterials in the environment: Behavior, fate, bioavailability, and effects. *Environ. Toxicol. Chem.* **2008**, *27*, 1825–1851. [[PubMed](#)]
54. Lützenkirchen, J.; Kupcik, T.; Fuss, M.; Walther, C.; Sarpola, A.; Sundman, O. Adsorption of Al-13-Keggin clusters to sapphire c-plane single crystals: Kinetic observations by streaming current measurements. *Appl. Surf. Sci.* **2010**, *256*, 5406–5411. [[CrossRef](#)]
55. Kersting, A.B. Plutonium Transport in the Environment. *Inorg. Chem.* **2013**, *52*, 3533–3546. [[CrossRef](#)]
56. Kersting, A.B.; Efur, D.W.; Finnegan, D.L.; Rokop, D.J.; Smith, D.K.; Thompson, J.L. Migration of plutonium in ground water at the Nevada Test Site. *Nature* **1999**, *397*, 56–59.
57. Altmaier, M.; Gaona, X.; Fanghänel, T. Recent Advances in Aqueous Actinide Chemistry and Thermodynamics. *Chem. Rev.* **2013**, *113*, 901–943. [[CrossRef](#)] [[PubMed](#)]
58. Morga, M.; Adamczyk, Z.; Kosior, D.; Oćwieja, M. Hematite/silica nanoparticle bilayers on mica: AFM and electrokinetic characterization. *Phys. Chem. Chem. Phys.* **2018**, *20*, 15368–15379. [[CrossRef](#)] [[PubMed](#)]
59. Morga, M.; Adamczyk, Z.; Basinska, T.; Komar, P.; Gosecka, M.; Żeliszewska, P.; Wasilewska, M. Spheroidal Microparticle Monolayers Characterized by Streaming Potential Measurements. *Langmuir* **2017**, *33*, 9916–9925. [[CrossRef](#)]
60. Oćwieja, M.; Maciejewska-Prończuk, J.; Adamczyk, Z.; Roman, M. Formation of positively charged gold nanoparticle monolayers on silica sensors. *J. Colloid Interface Sci.* **2017**, *501*, 192–201. [[CrossRef](#)]
61. Puzzo, D.P.; Bonifacio, L.D.; Oreopoulos, J.; Yip, C.M.; Manners, I.; Ozin, G.A. Color from colorless nanomaterials: Bragg reflectors made of nanoparticles. *J. Mater. Chem.* **2009**, *19*, 3500–3506. [[CrossRef](#)]
62. Makumire, S.; Chakravadhanula, V.S.; Köllisch, G.; Redel, E.; Shonhai, A. Immunomodulatory activity of zinc peroxide (ZnO₂) and titanium dioxide (TiO₂) nanoparticles and their effects on DNA and protein integrity. *Toxicol. Lett.* **2014**, *227*, 56–64. [[CrossRef](#)] [[PubMed](#)]
63. Selmani, A.; Špadina, M.; Plodinec, M.; Delač Marion, I.; Willinger, M.G.; Lützenkirchen, J.; Gafney, H.D.; Redel, E.A. Experimental and Theoretical Approach to Understanding the Surface Properties of One-Dimensional TiO₂ Nanomaterials. *J. Phys. Chem. C* **2015**, *119*, 19729–19742, Correction in **2016**, *120*, 4150. [[CrossRef](#)]
64. Vayssieres, L. On the thermodynamic stability of metal oxide nanoparticles in aqueous solutions. *Int. J. Nanotechnol.* **2005**, *2*, 411–439. [[CrossRef](#)]
65. Kasuga, T.; Hiramatsu, M.; Hoson, A.; Sekino, T.; Niihara, K. Formation of titanium oxide nanotube. *Langmuir* **1998**, *14*, 3160–3163. [[CrossRef](#)]
66. Sulpizi, M.; Lützenkirchen, J. Atypical titration curves for GaAl₁₂ Keggin-ions explained by a joint experimental and simulation approach. *J. Chem. Phys.* **2018**, *148*, 222836. [[CrossRef](#)]
67. Lützenkirchen, J. Unpublished results
68. Lützenkirchen, J.; Zimmermann, R.; Preočanin, T.; Filby, T.; Kupcik, T.; Küttner, D.; Abdelmonem, A.; Schild, D.; Rabung, T.; Plaschke, M.; et al. An attempt to explain bimodal behaviour of the sapphire c-plane electrolyte interface. *Adv. Colloid Interface Sci.* **2010**, *157*, 61–74.
69. Brkljača, Z.; Namjesnik, D.; Lützenkirchen, J.; Předota, M.; Preočanin, T. Quartz/Aqueous Electrolyte Solution Interface: Molecular Dynamic Simulation and Interfacial Potential Measurements. *J. Phys. Chem. C* **2018**, *122*, 24025–24036. [[CrossRef](#)]
70. Preočanin, T.; Namjesnik, D.; Brown, M.A.; Lützenkirchen, J. The relationship between inner surface potential and electrokinetic potential from an experimental and theoretical point of view. *Environ. Chem.* **2017**, *14*, 295–309. [[CrossRef](#)]
71. Lützenkirchen, J. Specific Ion. Effects at Two Single-Crystal Planes of Sapphire. *Langmuir* **2013**, *29*, 7726–7734.
72. Lützenkirchen, J.; Franks, G.V.; Plaschke, M.; Zimmermann, R.; Heberling, F.; Abdelmonem, A.; Darbha, G.K.; Schild, D.; Filby, A.; Eng, P.; et al. The surface chemistry of sapphire-c: A literature review and a study on various factors influencing its IEP. *Adv. Colloid Interface Sci.* **2018**, *251*, 1–25. [[CrossRef](#)] [[PubMed](#)]
73. Zhang, L.; Tian, C.; Waychunas, G.A.; Shen, Y.R. Structures and charging of alpha-alumina (0001)/water interfaces studied by sum-frequency vibrational spectroscopy. *J. Am. Chem. Soc.* **2008**, *130*, 7686–7694. [[CrossRef](#)]

74. Hiemstra, T.; Van Riemsdijk, W.H. A surface structural model for ferrihydrite I: Sites related to primary charge, molar mass, and mass density. *Geochim. Cosmochim. Acta* **2009**, *73*, 4423–4436. [[CrossRef](#)]
75. Preocanin, T.; Selmani, A.; Lindqvist-Reis, P.; Heberling, F.; Kallay, N.; Lützenkirchen, J. Surface charge at Teflon/aqueous solution of potassium chloride interfaces. *Colloids Surf. A-Physicochem. Eng. Asp.* **2012**, *412*, 120–128. [[CrossRef](#)]
76. Fatisson, J.; Domingos, R.F.; Wilkinson, K.J.; Tufenkji, N. Deposition of TiO₂ Nanoparticles onto Silica Measured Using a Quartz Crystal Microbalance with Dissipation Monitoring. *Langmuir* **2009**, *25*, 6062–6069. [[CrossRef](#)]
77. Wilhelm, P.; Stephan, D. On-line tracking of the coating of nanoscaled silica with titania nanoparticles via zeta-potential measurements. *J. Colloid Interface Sci.* **2006**, *293*, 88–92. [[CrossRef](#)]
78. Hintz, W.; Kleinschmidt, S.; Yordanova-Bineva, V.; Tomas, J. Surface-modification of Silica-particles by nano-scaled Titania-particles via Sol.-Gel-Process. In Proceedings of the World Congress on Particle Technology 6, WCTP6 2010, Nürnberg, Germany, 24–29 April 2010.
79. Bullard, J.W.; Cima, M.J. Orientation dependence of the isoelectric point of TiO₂ (rutile) surfaces. *Langmuir* **2006**, *22*, 10264–10271. [[CrossRef](#)]
80. Schmidt, M.; Wilson, R.E.; Lee, S.S.; Soderholm, L.; Fenter, P. Adsorption of Plutonium Oxide Nanoparticles. *Langmuir* **2012**, *28*, 2620–2627. [[CrossRef](#)]
81. Altmaier, M.; Neck, V.; Lützenkirchen, J.; Fanghänel, T. Solubility of plutonium in MgCl₂ and CaCl₂ solutions in contact with metallic iron. *Radiochim. Acta* **2009**, *97*, 187–192. [[CrossRef](#)]
82. Neck, V.; Altmaier, M.; Rabung, T.; Lützenkirchen, J.; Fanghänel, T. Thermodynamics of trivalent actinides and neodymium in NaCl, MgCl₂, and CaCl₂ solutions: Solubility, hydrolysis, and ternary Ca-M(III)-OH complexes. *Pure Appl. Chem.* **2009**, *81*, 1555–1568. [[CrossRef](#)]
83. Lützenkirchen, J. Surface complexation models of adsorption: A critical survey in the context of experimental data. *Surfactant Sci. Ser.* **2002**, *107*, 631–710.
84. Abbas, Z.; Labbez, C.; Nordholm, S.; Ahlberg, E. Size-dependent surface charging of nanoparticles. *J. Phys. Chem. C* **2008**, *112*, 5715–5723. [[CrossRef](#)]
85. Vayssieres, L. On the Effect of Nanoparticle Size on Water-Oxide Interfacial Chemistry. *J. Phys. Chem. C* **2009**, *113*, 4733–4736. [[CrossRef](#)]



© 2020 by the authors. Licensee MDPI, Basel, Switzerland. This article is an open access article distributed under the terms and conditions of the Creative Commons Attribution (CC BY) license (<http://creativecommons.org/licenses/by/4.0/>).